NGU REPORT 2013.030

Compilation of various airborne geophysical data in the Oslofjord area

GEOLOGY FOR SOCIETY

SINCE 1858

GEOLOGICAL SURVEY OF NORWAY

- NGU -

NORGES GEOLOGISKE UNDERSØKELSE
· NGU ·

REPORT

Geological Survey of Norway
P.O.Box 6315 Sluppen
NO-7491 TRONDHEIM
Tel.: 47 73 90 40 00

Report no.: 2013.030

ISSN: 0800-3416 (print)
ISSN: 2387-3515 (online)

Grading: Open

Title:
Compilation of various airborne geophysical data in the Oslofjord area

Authors:
Vikas Baranwal

Client:
NGU

County:
Akershus, Buskerud, Oppland, Oslo, Vestfold and Østfold

Commune:
Several

Map-sheet name (M=1:250.000)
OSLO, HAMAR and SKIEN

Map-sheet no. and -name (M=1:50.000)
Several

Deposit name and grid-reference:

Number of pages: 38
Map enclosures:

Price (NOK): 150,-

Fieldwork carried out:
1981 - 2011

Date of report:
27.08.2015

Project no.:
353200

Person responsible:
Jan S. Rønning

Summary:

NGU has been acquiring airborne data in the Oslofjord area from early eighties until 2011. Some of the airborne surveys were performed by NGU itself and some of them were contracted to surveying companies e.g. Fugro, SGU. These airborne data were presented in various reports and stored as separate grids and databases for individual surveys. Later, it seemed necessary to compile this data together and present them as a single grid data. Therefore, various grids for magnetic and radiometric data were stitched together from airborne surveys performed during 1981-2011. Stitching of magnetic data was straightforward. It was done by suture method of grid knitting available in Geosoft software. However, stitching of radiometric data could not be stitched automatically because some of earlier surveys were not calibrated. Some of the surveys had only counts of gamma radiations for K, eU and eTh windows as gridded data. So scatter plot of the overlapping areas of various grids was made and regression analysis was performed to get slope and intercept of the fitting line. The regression parameters were used to bring two grids at similar level of ground concentration and then all the grids were stitched together one by one to get the final stitched grid.

The scatter analysis didn't give always a good linear relation especially between NGU and Fugro data for uranium. Sometime there were not sufficient overlapping areas and parameters of regression analysis could be inaccurate. Quality of the stitched grids for Magnetic anomaly is quite good and no boundaries and along-line errors are visible. Quality of stitched radiometry grids are good except some areas where along-line leveling errors could not be removed in the original grid. A critical review of the individual radiometry maps indicate minor level errors from one grid to other on all three elements, and some along-line level errors within Siljan, Hurdal survey areas. Re-processing of the data with correct coefficients and thorough leveling is required to get further improvement in the quality of stitched grid. NGU grid was around 1.6 times higher in concentration of potassium and around 1.3 times higher in concentration of thorium in the overlapping areas of SGU and Fugro grids. Uranium was found 1.3 times higher in NGU grid than SGU. However, Fugro grid could not give a good linear relationship with NGU grid for uranium. Some of the survey area showed a higher concentration compared to neighboring areas in the stitching then parameters from other survey area performed in the same year were used.

Keywords:	Geophysics	Compilation
Stitching	Radiometry	Magnetic
Airborne	Oslofjord area	Scientific report

CONTENTS

FIGURES

TABLES

1. INTRODUCTION

Many airborne geophysical surveys were performed in the Oslofjord area from early eighties until present. The objective of the airborne geophysical surveys is primarily to obtain a dense high-resolution magnetic, electromagnetic and radiometric data over the survey area for geological mapping. Such mapping assists geologists and geophysicists in various types of the geological and environmental studies e.g. bedrock mapping, mineral prospecting, radon contamination, heat production, tunnel construction, clay characterization and groundwater explorations. The airborne geophysical data is required for the enhancement of a general understanding of the regional geology of the area. In this regard, the data can be used to map contacts and structural features. It improves defining the potential of known zones of mineralization, their geological settings, and identifying new areas of interest. Acquired data can be used for foreseeing possible tunnel construction problems, deep weathering, and evaluation of possible radon problems in houses and characterization of soft sediments.

Gridded data and databases were presented in individual reports from these surveys and stored digitally. However, to have an overview of the larger areas all together, compilation of these data in single grids was necessary. A mosaic or simple alignment of the grids would not solve the purpose because level difference would always be present in various surveys due to different calibration parameters and processing strategies. Therefore magnetic and radiometry data collected from various surveys during 1981-2011 were stitched together in single grids using Geosoft routines and some statistical analysis.

2. LOCATION

The area of interest is located around the Oslofjord. Fixed-wing airborne surveys were performed in relatively flat and large areas to collect mostly magnetic and radiometry data. However, helicopter-borne surveys were performed in relatively smaller parts to cover more rough terrain areas with mineral prospecting potentials. Detailed frequency-domain EM data were collected in addition to magnetic and radiometry data in most of helicopter-borne survey. Surveys were performed in different years as shown in Fig. 1. Boundaries with colors as black, green, red and blue show surveys before 2005 by helicopter and fix-wing, in 2006 by helicopter only, in 2009 by fix-wing only and in 2010-2011 by helicopter only, respectively. Details of the survey type, collected data, year of measurements, line-spacing, line direction, area of survey and corresponding reports are summarized in tables 1 and 2. Mag, Rad, VLF-EM, Cx, and Cp represent Magnetic, Radiometric, Very Low Frequency Electromagnetic, Co-axial EM and Co-planar EM data, respectively.

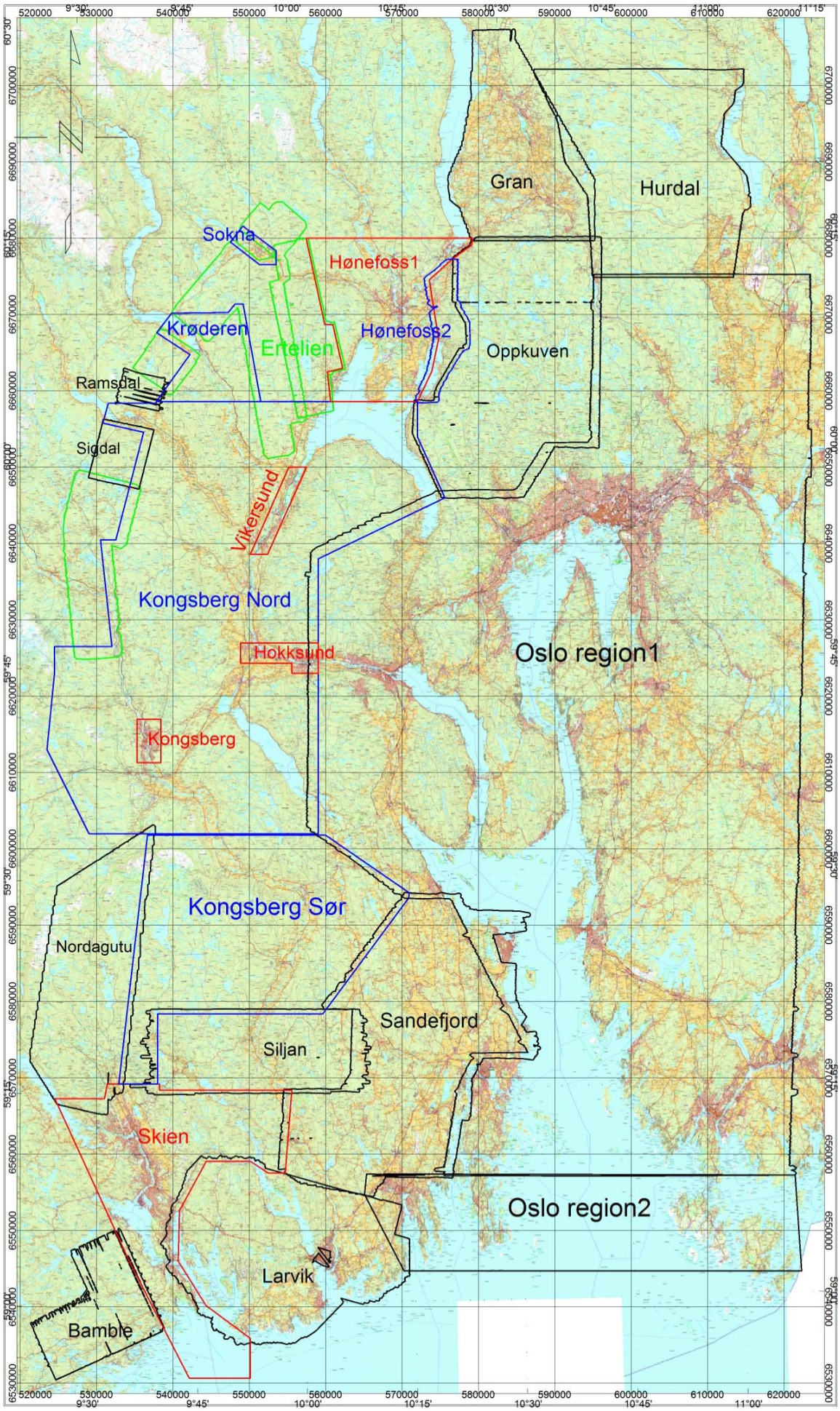

Figure 1: Location of the helicopter and fixed-wing surveys in the Oslofjord area (from Baranwal et al., 2013a). Details of the surveys are given in tables 1 and 2.

Table 1: Description of the helicopter-borne surveys around the Oslofjord area. See text for details of the abbreviations.

Survey area	Year of Survey	Line spacing (m) and direction	Aircraft elevation (m)	Survey area (km^2)	Type of collected data	References
Helicopter-borne surveys						
Siljan	1981	200 E-W	60	300	Mag, Rad, VLF, Cx: 1000 Hz	Håbrekke, 1982
Oppkuven	1997-1999	200 E-W	80	832	Mag, Rad, VLF, Cp: 4300 & 32100 Hz, Cx: 900 & 4500 Hz	Beard, 1998 Beard & Rønning, 1997 Beard & Lutro, 2000
Gran	1997	200 N-S	80	404	Mag, Rad, VLF	Beard, 1998
Larvik	1997-1998	100 NE-SW, 150 N75W-S75E	60 & 80	600	Same as above	Mogaard, 1998 Beard, 1999
Nordagutu	1999	200 N-S	60	385	Mag, Rad, VLF, Cp: 880, 6606 & 34133 Hz, Cx: 980 & 7001 Hz	Mogaard & Beard, 2000
Sandefjord	2000	200 E-W	60	690	Same as above	Mogaard, 2001
Hurdal	2000	200 E-W	60	556	Same as above	Beard and Mogaard, 2001
Bamble Sigdal & Ramsdal Ertelien	2005-2006	100 N24W-S24E 100 N78E-S78W 100 N78W-S78E	60	145 250 110	Mag, Cp: 880, 6606 & 34133 Hz, Cx: 980 & 7001 Hz	Mogaard, 2006
Kongsberg Nord & Sør Krøderen, Sokna and Hønefoss2	2009 - 2011	200 E-W	60	2800	Mag, Rad, Cp: 880, 6606 & 34133 Hz, Cx: 980 & 7001 Hz	Baranwal et al., 2013b

Table 2: Description of the fixed-wing surveys around the Oslofjord area. See text for details of the abbreviations.

Survey area	Year of Survey	Line spacing (m) and direction	Aircraft elevation (m)	Survey area (km^2)	Type of collected data	References
Fixed-wing surveys						
Oslo region 1& 2 **(Fugro grids)**	2003	250 & 500 E-W	60 & 100	6000	Mag, Rad & VLF	Fugro, 2003
Skien, Kongsberg, Hokksund, Virkesund, Hønefoss1	2009	200 E-W	60	980	Mag, Rad & VLF	SGU, 2009

3. AIRBORNE SURVEYS EQUIPMENT

Both the fixed-wing and helicopter-borne surveys collected electromagnetic, magnetic and radiometric data. A cesium vapor magnetometer is generally used to measure total magnetic field and a Sodium Iodide (NAI) detector with either 256 or 1024 channels was used to register natural gamma-radiations. After processing, the magnetic data are presented as total magnetic field anomaly map and radiometry data as ground concentration of naturally occurring radioactive elements e.g. potassium (K), equivalent uranium (eU), equivalent thorium (eTh). Different types of EM data were also collected depending on the EM equipments used in these surveys however EM data grids are not presented and stitched. Helicopter-borne surveys performed before 2005 collected VLF EM data in addition to frequency-domain EM data. VLF EM measurements were stopped after 2003. Frequency-domain Helicopter-borne ElectroMagnetic (FHEM) data before 1999 were collected for four frequencies, 4.3 & 32.1 kHz in horizontal co-planar setting and 900 Hz & 4.5 kHz in vertical co-axial setting of transmitter-receiver coil set. From year 2000 onwards, a five-frequency EM system Hummingbird^{TM} (880 Hz, 6.6 kHz and 34.1 kHz in horizontal coplanar setting; 980 Hz and 7 kHz in vertical co-axial setting) were used. This report is basically aimed to present a complication of the existing data and grids obtained from various airborne surveys in Oslofjord area, therefore details of the instrumentation, data acquisition and data processing are not discussed in this report. Details of those parameters can be found from various reports referred in the tables 1 and 2. EM data is not presented in this report.

4. COMPILATION OF AIRBORNE GEOPHYSICAL DATA

VLF and frequency-domain EM were not well processed from earlier surveys. All the airborne EM data could have been re-processed but then correct calibration parameters from those surveys were needed to perform inversion to obtain true resistivity of the subsurface. Such details were poorly recorded in the reports and sometime raw data was also missing. These limitations made compilation of electrical resistivity map from airborne EM data very challenging and difficult. Compilation of airborne EM data was not primary concern therefore compilation of resistivity maps of the area was not attempted. In this work, only compilation and stitching of magnetic data and radiometric data (K, eU and eTh) were performed.

4.1 Data description

Airborne data from the northern and southwestern parts of the area were acquired by helicopter survey conducted by the Geological Survey of Norway (NGU) during the time period 1981-2011. The pattern of flight lines was generally along E-W direction except for the Gran survey that was flown in N-S direction. Generally, the nominal line spacing and flight altitude were 200 m and 60 m, respectively. Gamma-ray spectrometer was attached under the belly of helicopter while magnetic sensor was in a bird towed at 30 m below helicopter. In some earlier surveys e.g. in Nineties and also in some surveys where no EM data were collected then a smaller bird containing only magnetic sensor was towed at 15 m below the helicopter. Fugro Airborne Surveys (2003) carried out a larger fixed wing survey under a project GEOS of ca. 24.000 km to cover the relatively flat areas to the east and north of Oslofjord (Oslo region-1 in Fig. 1). The flight altitude was here 60 m and 100 m in rural and urban areas, respectively. The line spacing was ca. 250 m. A relatively small area in the outer part of Oslofjord (Oslo region-2 in Fig. 1) was flown with a line spacing of 500 m. Some areas in the west side were surveyed by Geological Survey of Sweden (SGU, 2009) using a fixed wing aircraft at 200 m line spacing in E-W direction and approx. 60 m altitude. In these surveys, all instruments were fixed on the aircraft.

Earlier processed magnetic data were stored and gridded either as total magnetic field or magnetic anomaly. A mosaic of pre-stitched magnetic and radiometry data are shown in Figs. 2-5. Magnetic data were processed to generate total magnetic field and magnetic anomaly from surveys performed before year 2003 (white boundary of surveys in Fig. 2) and after year 2003 (black boundary of surveys in Fig. 2), respectively. Radiometry data were processed to generate ground concentration of K, eU and eTh from surveys after year 1998 (black boundary of surveys in Figs. 3-5). Before year 1998, radiometry data were available as counts/second (c/s) from energy windows of K, eU and eTh (white boundary of surveys in Figs. 3-5). Radiometry data from Siljan were only background radiation corrected however data from Larvik, Gran and Oppkuven were background corrected, stripped for back scatter and height corrected.

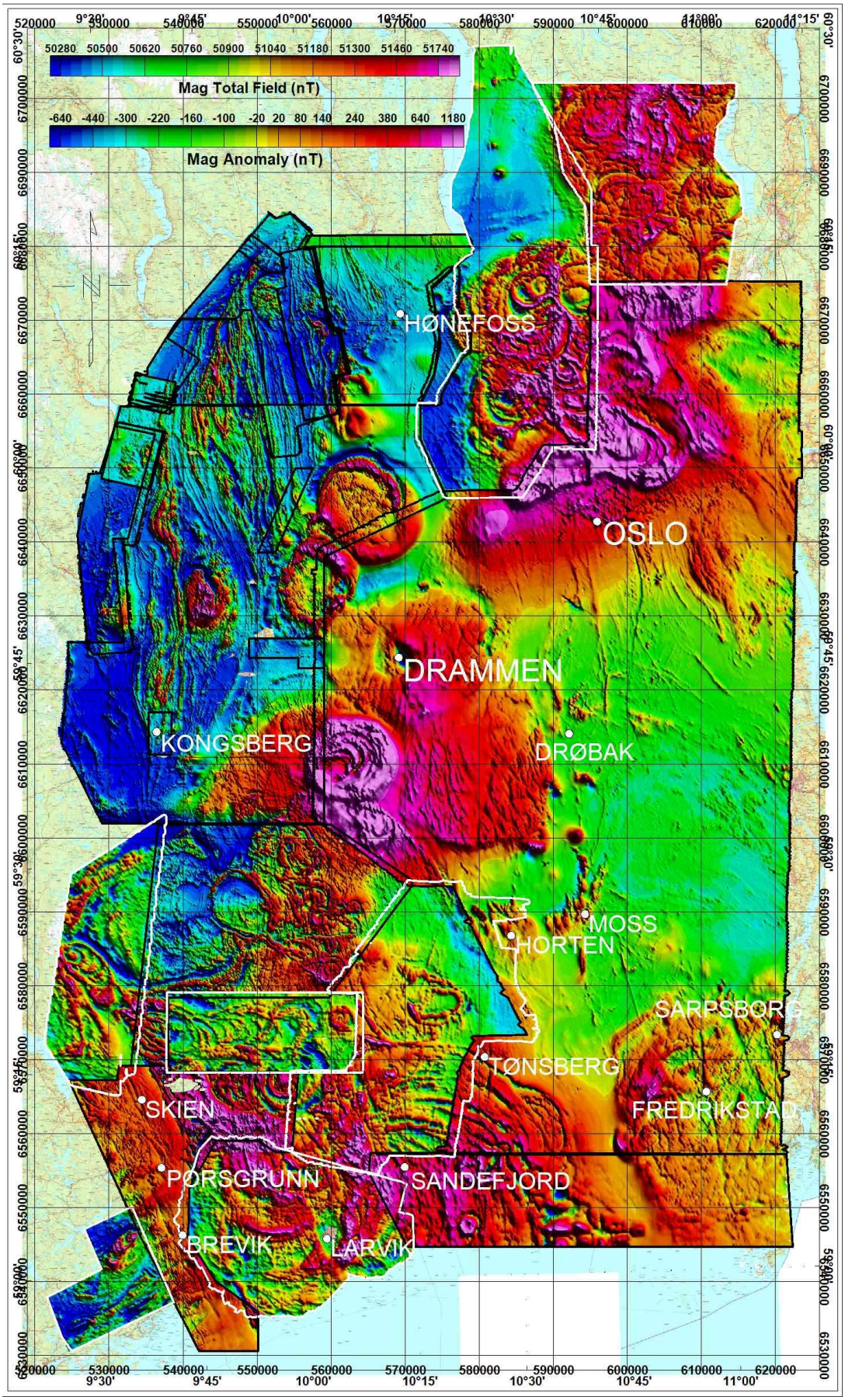

Figure 2: Mosaic of magnetic data before stitching from Oslofjord area. Pre-stitching data were available as total magnetic field and magnetic anomaly from survey areas marked with white and black boundaries, respectively.

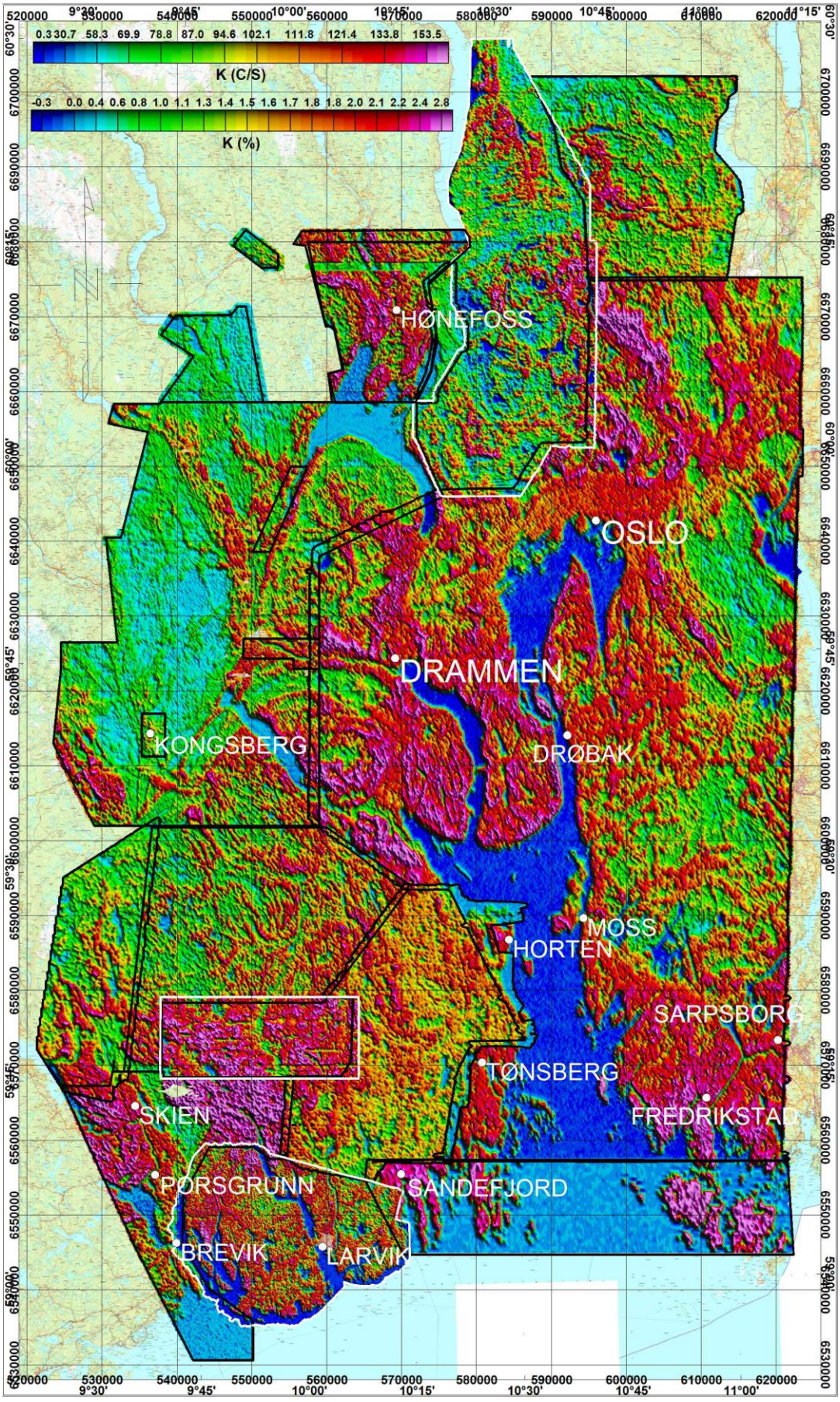

Figure 3: Mosaic of potassium before stitching from Oslofjord area. Pre-stitching data were available as counts/second (c/s) and ground concentration in % from survey areas marked with white and black boundaries, respectively.

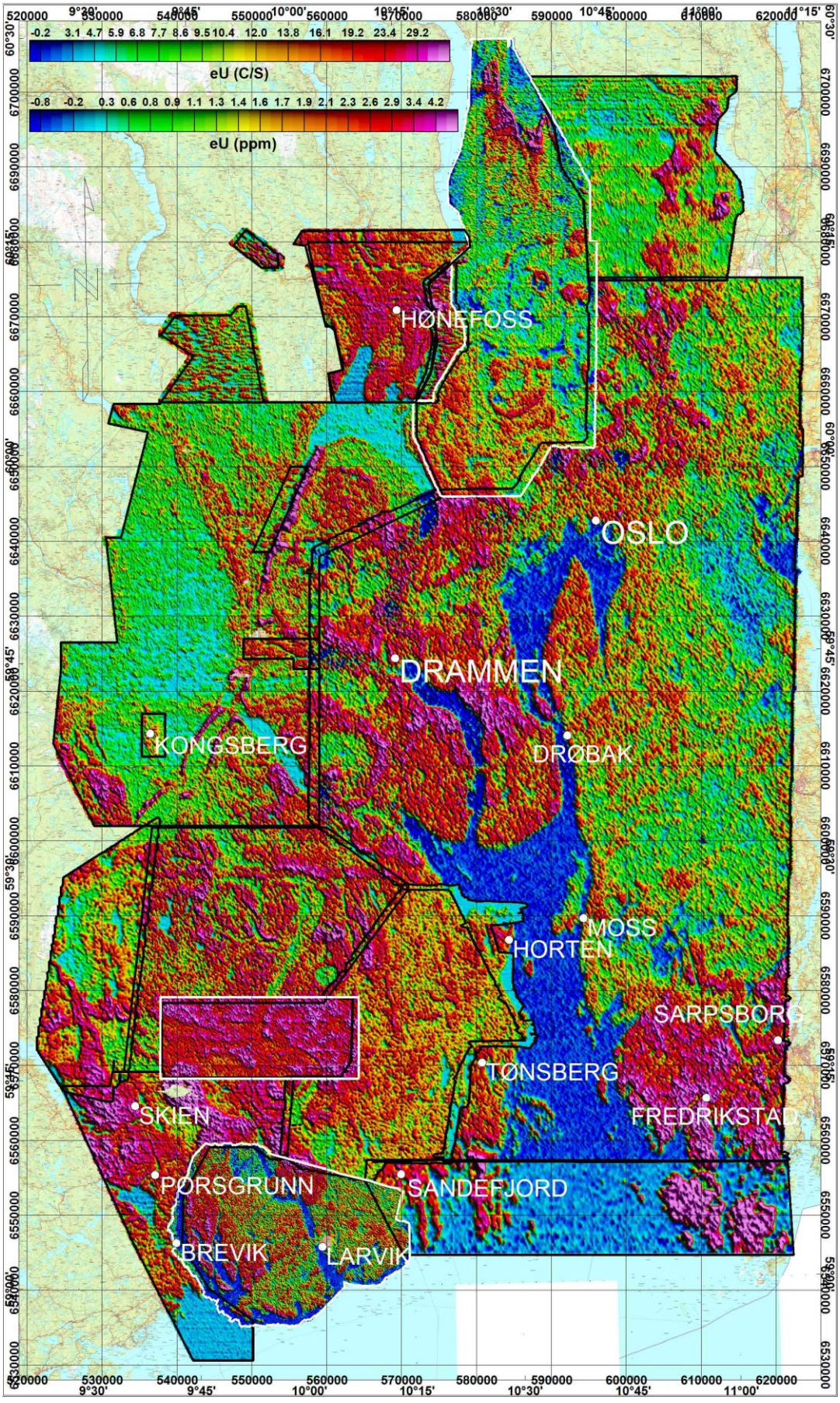

Figure 4: Mosaic of uranium before stitching from Oslofjord area. Pre-stitching data were available as counts/second (c/s) and ground concentration in ppm from survey areas marked with white and black boundaries, respectively.

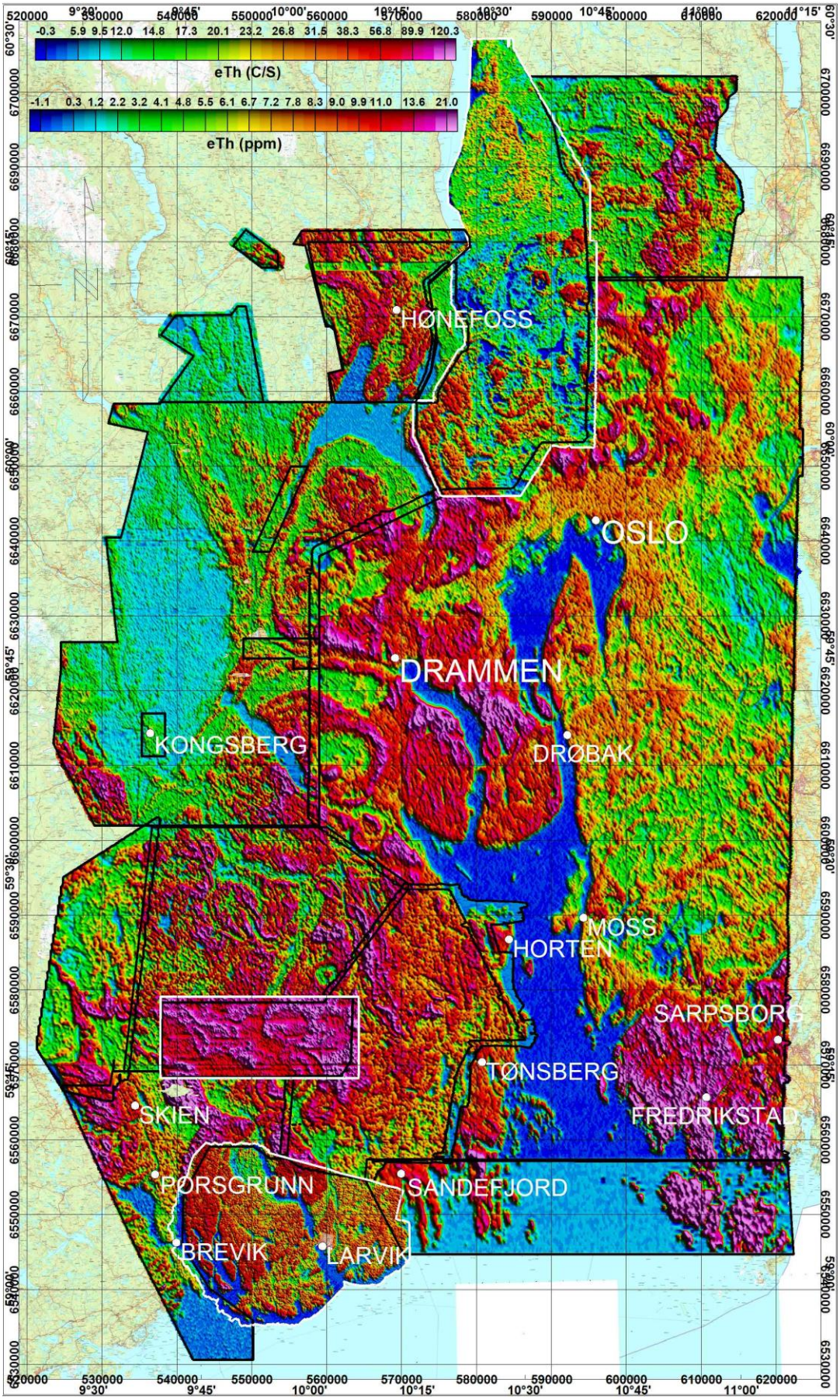

Figure 5: Mosaic of thorium before stitching from Oslofjord area. Pre-stitching data were available as counts/second (c/s) and ground concentration in ppm from survey areas marked with white and black boundaries, respectively.

4.2 Compilation of airborne magnetic data

There were various options available for stitching of the grids in Geosoft but we found the suture method using overlapping points to calculate the static trend as most suitable for the continuation and smoothness of the overlapping areas of the grids. Two grids were stitched together making first grid as a basis and keeping unchanged while a static trend was removed from the second grid.

Magnetic data collected after 2003 were well processed and corrected for diurnal and IGRF. However magnetic data collected before were only corrected for diurnal corrections. Because there was a sensor height difference between fix-wing and helicopter-borne surveys, the processed data from fix-wing surveys were downward continuated using a frequency-domain filtering package (Geosoft, 2010a) from an altitude of 60 meters to 30 meters before stitching. The downward continuation brought both fix-wing airborne magnetic data collected at approximately 60 m height and helicopter-borne magnetic data collected at approximately 30 m height at the same level. Some of the grids were re-processed and micro-leveled as required. The total magnetic field anomaly grid from Kongsberg Nord was taken as a base or starting grid and stitching was performed with adjacent/overlapping areas from other surveys. Two grids were stitched together at a time by removing static trend from second grid and keeping first grid unchanged using suture method of Gridknit (Geosoft, 2010b). Next grid was then stitched with the earlier stitched grid and same process was continued until all the grids were stitched one by one. The final grid with cell size 50 x 50 meters of the magnetic anomaly is shown in Fig. 6. The magnetic data was stitched quite well without any visible error and differences at the boundaries. Vertical derivative, horizontal gradient, analytic signal and Tilt derivative from the finally stitched total magnetic field anomaly grid were calculated using Fast Fourier Transform (FFT) and Convolution tools available in Geosoft. These maps can be provided on request.

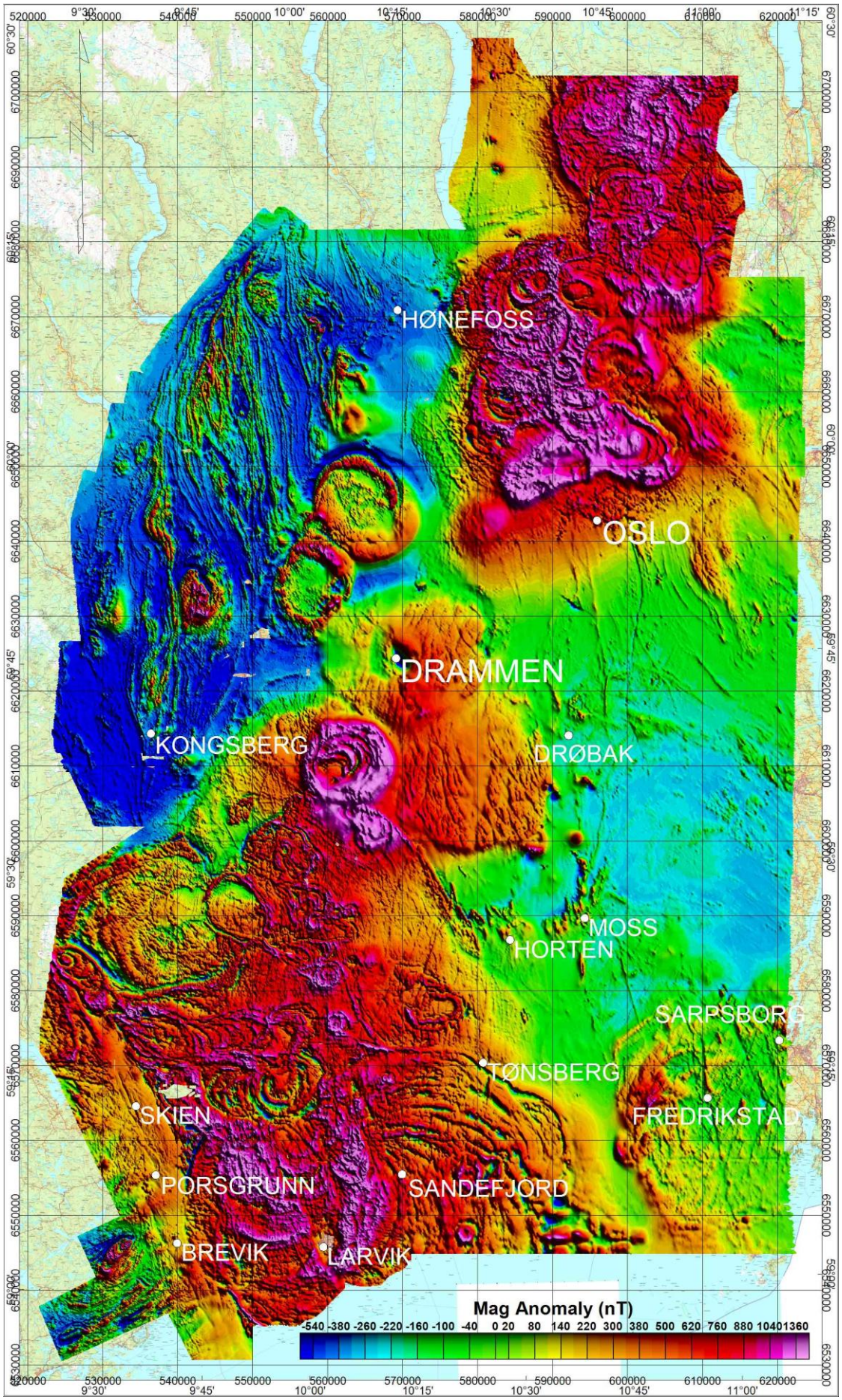

Figure 6: Stitched magnetic anomaly map from the Oslofjord area.

4.3 Correction and stitching of airborne radiometric data

Compilation of radiometric data i.e. stitching of K, eU and eTh grids was not as straightforward as the magnetic. Some of the old surveys were not calibrated at all and only counts/second (c/s) from energy window of three radio-elements (K, eU and eTh) were provided. In some other surveys, calibration was done and ground concentration was calculated but there were level differences in the concentrations from the two surveys in the overlapping areas. Some of the grids had along-line errors so some efforts were made to micro-level them as required (e.g. Larvik, Hurdal etc.). The radiometric surveys were divided in three groups as surveys performed by NGU during 2009-2011 to be called NGU grids, surveys performed by SGU in 2009 to be called as SGU grids and a large area surveyed by Fugro using fixed wing in 2003 (Fugro, 2003) to be called as Fugro grids.

Fugro had processed radiometry data with "Noise Adjusted Singular Value Decomposition" (NASVD) method as well (Minty & McFadden, 1998). They provided concentrations of K, eU and eTh grids without NASVD and with NASVD. Concentrations obtained with NASVD from Fugro survey matched better with concentrations of SGU and NGU surveys though NGU and SGU had not performed NASVD over their data. Details of the airborne radiometry survey year and types of processed data available are mentioned in table 3. Table 3 also contains regression parameters from scatter analysis and sequence of the grid stitching (discussed in detail in following section). First, all the grids surveyed by NGU in 2009-2010 (Kongsberg Nord, Sokna, Krøderen, Hønefoss2) were mosaiced and then stitched together with NGU grid in 2011 (Kongsberg Sør) by removing static trend from 2009-2010 mosiaced grids and using suture method of Gridknit (Geosoft, 2010b). Kongsberg Sør grid was assumed as basis and kept unchanged however mosaic of NGU grids from 2009-2010 were allowed to change. All the SGU grids were from same surveys so they were made just a mosaic for further correction based on the scatter analysis. Stitching of rest of the grids always followed two steps of stitching the two grids at a time 1) regression parameters from scatter analysis of overlapping areas of two grids were used to correct the second grid then 2) suture method of Gridknit was used to remove static trend from the second grid however first grid kept unchanged. This process was repeated again to the next grid until all the grids were stitched together.

4.3.1 Scatter analysis of overlapping grids and stitching

Scatter analysis was performed to see the relationship among various radiometry surveys data. Overlapping areas of two neighboring surveys were stored in a database and two scatter plots were made by plotting one of the surveys data at x-axis and other survey data at y-axis and vice-versa. A regression line was fitted to obtain the linear relationship between these two surveys data. Fig. 7 shows scatter plot between NGU and Fugro data for potassium. In Fig. 7a, regression minimized the distance w.r.t. NGU data to get a best fit (Fig. 7a, Fugro data on x-axis and NGU data on y-axis). In Fig. 7b, plotting was reversed on the axes (Fig. 7b, Fugro data on y-axis and NGU data on x-axis) then regression minimized the distance w.r.t. Fugro data. Because, the distribution of data was not symmetric along the sides of regression line therefore these two regression lines were different to each other. Parameters of two regression lines were not equivalent (i.e. slope in Fig. 7a was not inverse of slope in Fig. 7b and intercept was not negative of intercept divided by the slope) as shown in equations of the Fig. 7. Therefore one of the fitting was preferred over the other by visual inspection in which regression line passed through more data

and fitting was perceived more appropriate. These regression parameters (e.g. parameters of Fig. 7a in this case to correct Fugro grid) were used for modifying one of the grids. Similar scatter plots were plotted for uranium and thorium as shown in Figs. 8 and 9.

Table 3: Available radiometry data, survey year, correction parameters and sequence of the grid stitching.

Survey area	Year	Status of old data and grids	Correction factors from scatter analysis			Sequence of radiometry grid stitching
			K	eU	eTh	
NGU grids			**Regression parameters**			(Grids were modified using regression parameters)
			Slope Intercept	**Slope Intercept**	**Slope Intercept**	
Kongsberg Sør	2011	K (%), eU (ppm), eTh (ppm)	-	-	-	Grid stitching was started with this grid as basis.
Kongsberg Nord, Sokna, Krøderen, Hønefoss2	2009-2010	Same as above	1 0	1 0	1 0	Made a mosaic together and then stitched with Kongsberg Nord grid
SGU grids						
Hønefoss1, Virkersund, Hokksund Kongsberg Skien	2009	Same as above	0.58 0.39	0.75 0	1/1.31 -0.71/1.31	Made a mosaic together and modified the grid
Oslo region1 & 2 **(Fugro grids)**	2003	K (%), eU (ppm), eTh (ppm) using NASVD	0.61 0.5	-	0.78 0.64	Made a mosaic together and modified the grid, stitched with NGU and SGU grids
Larvik	1997-1998	K, eU, eTh windows at 60 m height in c/s	0.019 -0.015	0.16 0.44	0.36 -1.68	Modified the grid, stitched with above grid
Oppkuven, Gran	1997	Same as above	0.016 0.198	0.16 0.44	0.27 0.58	Same process as mentioned above
Sandefjord	2000	K (%), eU (ppm), eTh (ppm)	1.41 -0.30	1/0.51 -0.71/0.51	1.16 -1.55	Same process as mentioned above
Nordagutu	1999	Same as above	1.42 -0.40	1/0.64 -0.50/0.64	1.16 -0.71	Same process as mentioned above
Hurdal	2000	Same as above	1.10 1.41	1/0.51 -0.71/0.51	0.88 0.92	Same process as mentioned above
Siljan	1981	K, eU, eTh windows in c/s	0.013 0.360	0.17 -1.44	0.25 -13.50	Same process as mentioned above

Modified grid was calculated using equation (1) and regression parameters of scatter analysis as given below

$$\boldsymbol{Grid_{mod} = Slope \times Grid + Intercept} \quad \ldots(1)$$

where $Grid_{\mathrm{mod}}$ was modified grid, $Grid$ was original grid to be corrected. $Slope$ and $Intercept$ were obtained from regression analysis of the scatter plot (see table 3).

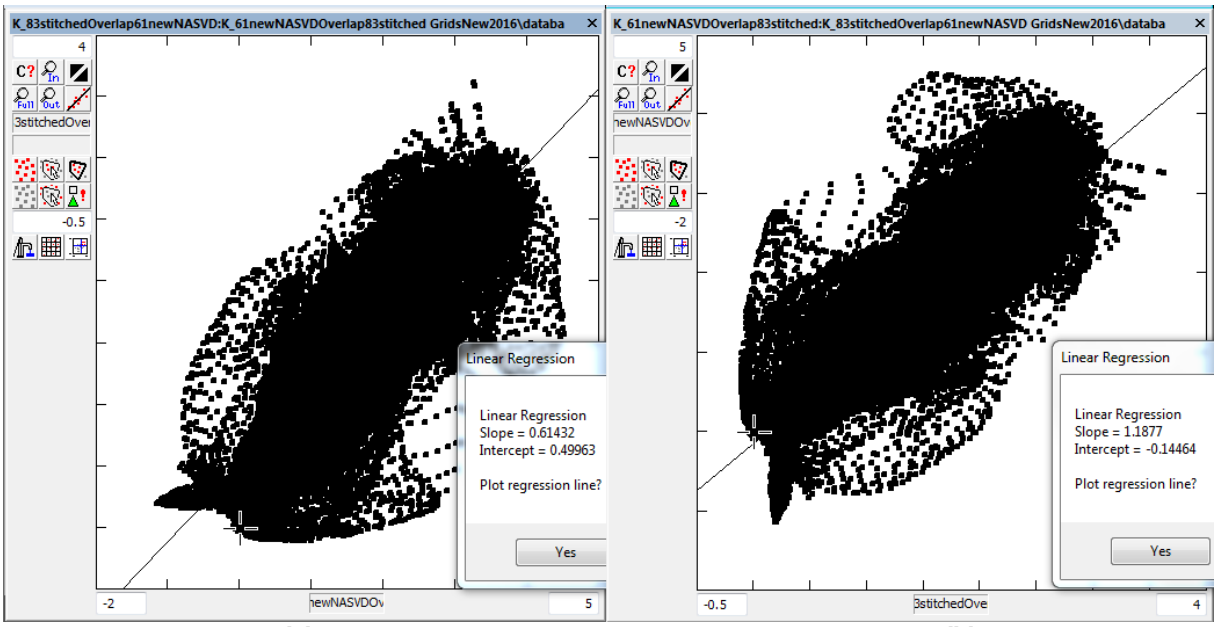

(a) **(b)**

Figure 7: Scatter plot for potassium between overlapping areas of stitched NGU grid and Fugro grid with (a) NGU grid on y-axis and Fugro grid on x-axis and (b) vice-versa

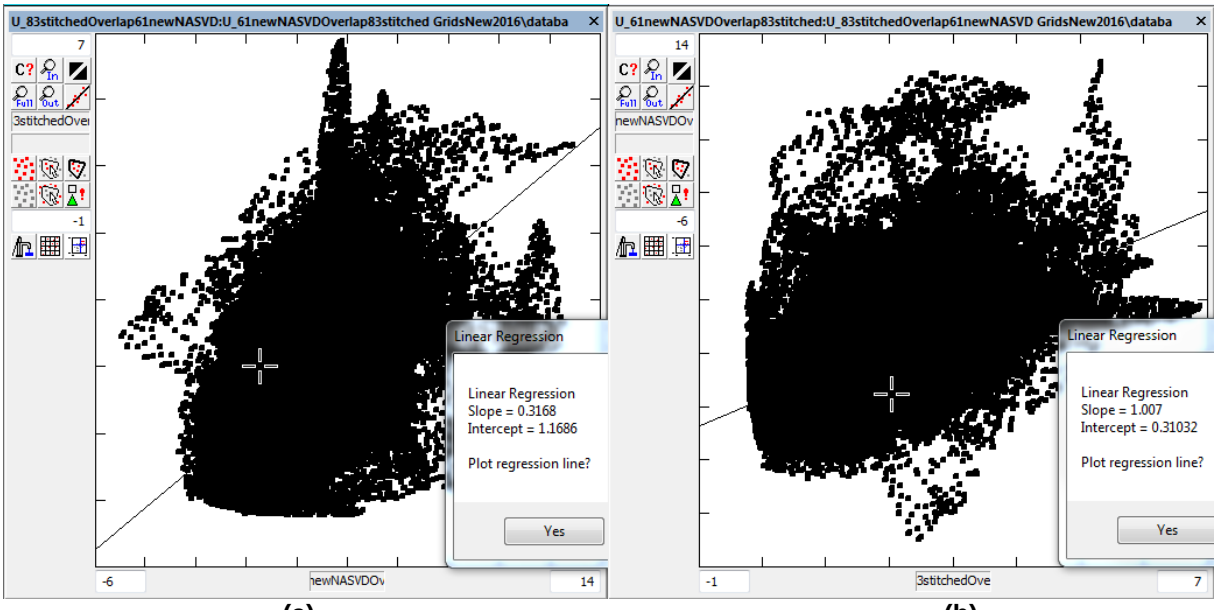

(a) **(b)**

Figure 8: Scatter plot for uranium between overlapping areas of stitched NGU grid and Fugro grid with (a) NGU grid on y-axis and Fugro grid on x-axis and (b) vice-versa

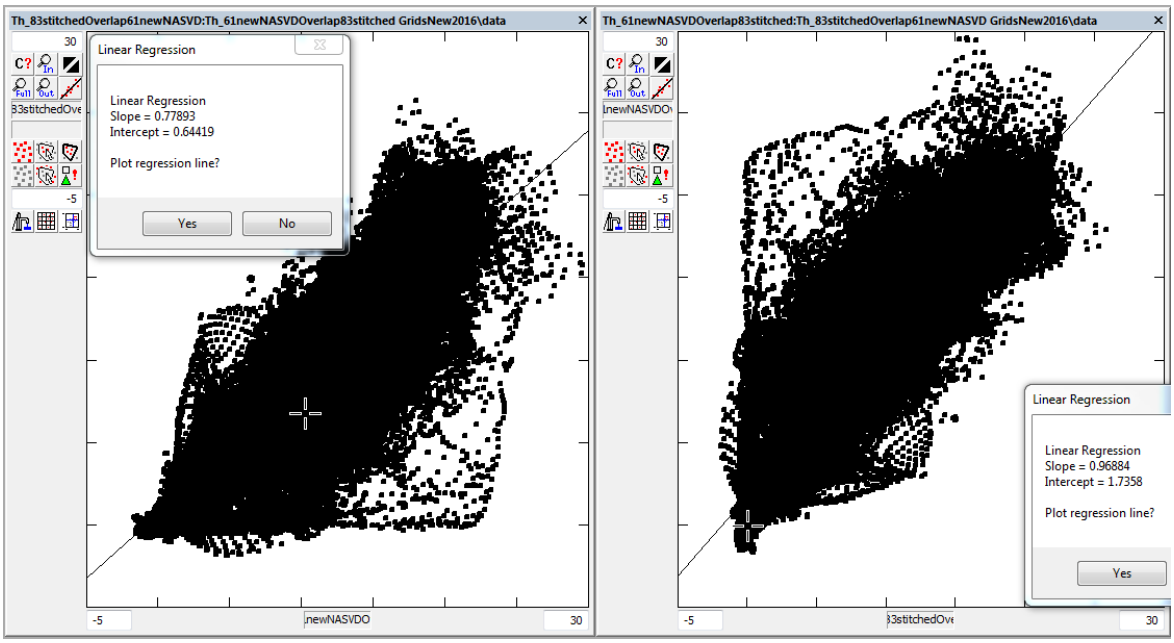

(a) **(b)**

Figure 9: Scatter plot for thorium between overlapping areas of stitched NGU grid and Fugro grid with (a) NGU grid on y-axis and Fugro grid on x-axis and (b) vice-versa

There were two options in Geosoft to calculate the trend to be removed from one of the grids 1) static as a constant value and 2) slope as varying value along a plane. Both of these methods and modification of the Fugro grid using both of the regression lines for potassium and uranium (Figs. 7 and 8) were tested by comparing the values along two perpendicular profiles lines (L2 and L3) as shown in Fig. 10.

Generally, potassium and thorium shows less noise in the data in comparison to uranium which is affected by radon. Thorium window also does not have back-scattered radiation as being highest energy peak compared potassium and uranium therefore plots of potassium and uranium are only shown here and thorium is not shown. Profile lines L2 and L3 are shown by black coloured lines in Fig. 10. Boundaries of stitched NGU grid and Fugro grid are shown by blue and red colours, respectively. Stitching of these two grids for potassium and uranium was performed using static and slope methods of grid knitting keeping NGU grid unchanged and allowing changes in Fugro grid. Suture path of the automatic stitching process passed through middle of the overlapping areas of the two grids and shown by green colour. Fugro grid was modified by regression parameters obtained from Figs. 7a and Fig. 8a for potassium and uranium, respectively and named as "calculated 1". Similarly, Fugro grid was modified by other regression parameters shown in Figs. 7b and Fig. 8b and named as "calculated 2". Grid data from all these five types of grids (mosaic, static, slope, "calculated 1", and "calculated 2") were profiled along lines L2 and L3 and plotted in Fig. 11. Slope method of stitching resulted in maximum change in the data (green coloured in Fig. 11) and very sensitive to any changes in the data. Stitched grid using slope method changed a lot from one to other regions and some unrealistic jumps in the grid were observed. However, other methods showed rather smoother variation w.r.t. mosaiced grid data (i.e. actual grid value shown by blue colour) except "calculated 1" uranium values (purple coloured line in eU plots of Fig. 11). "Calculated 1" uranium values were very low because uranium data of NGU and Fugro grids had a poor linear relation and regression in Fig. 8a resulted in a slope of 0.3 which was too small to be realistic.

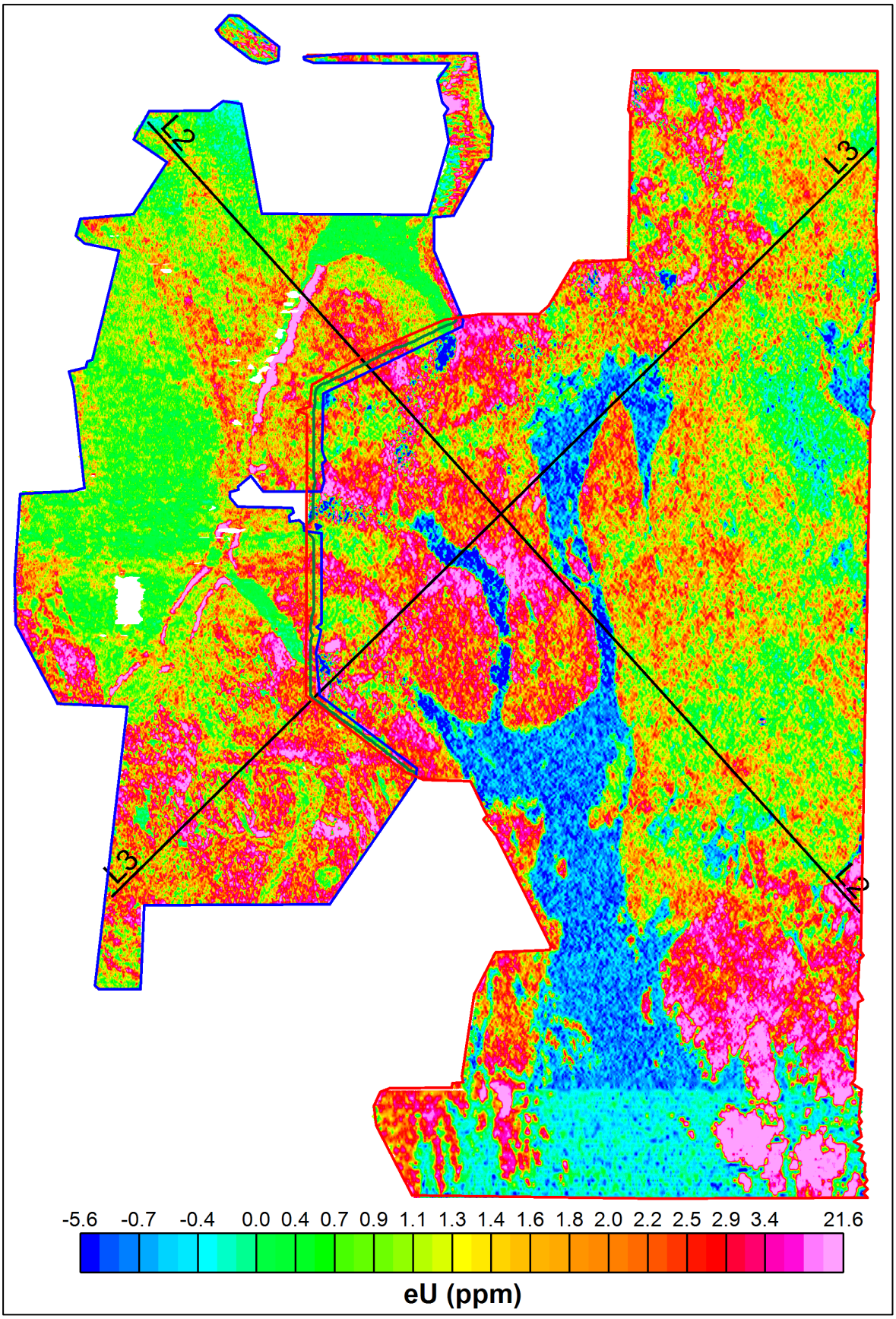

Figure 10: Plot of profile lines L2 and L3 (black) and automatic suture path (green) of the grid knitting over mosaiced uranium grid from NGU and Fugro surveys with their boundaries (blue and red).

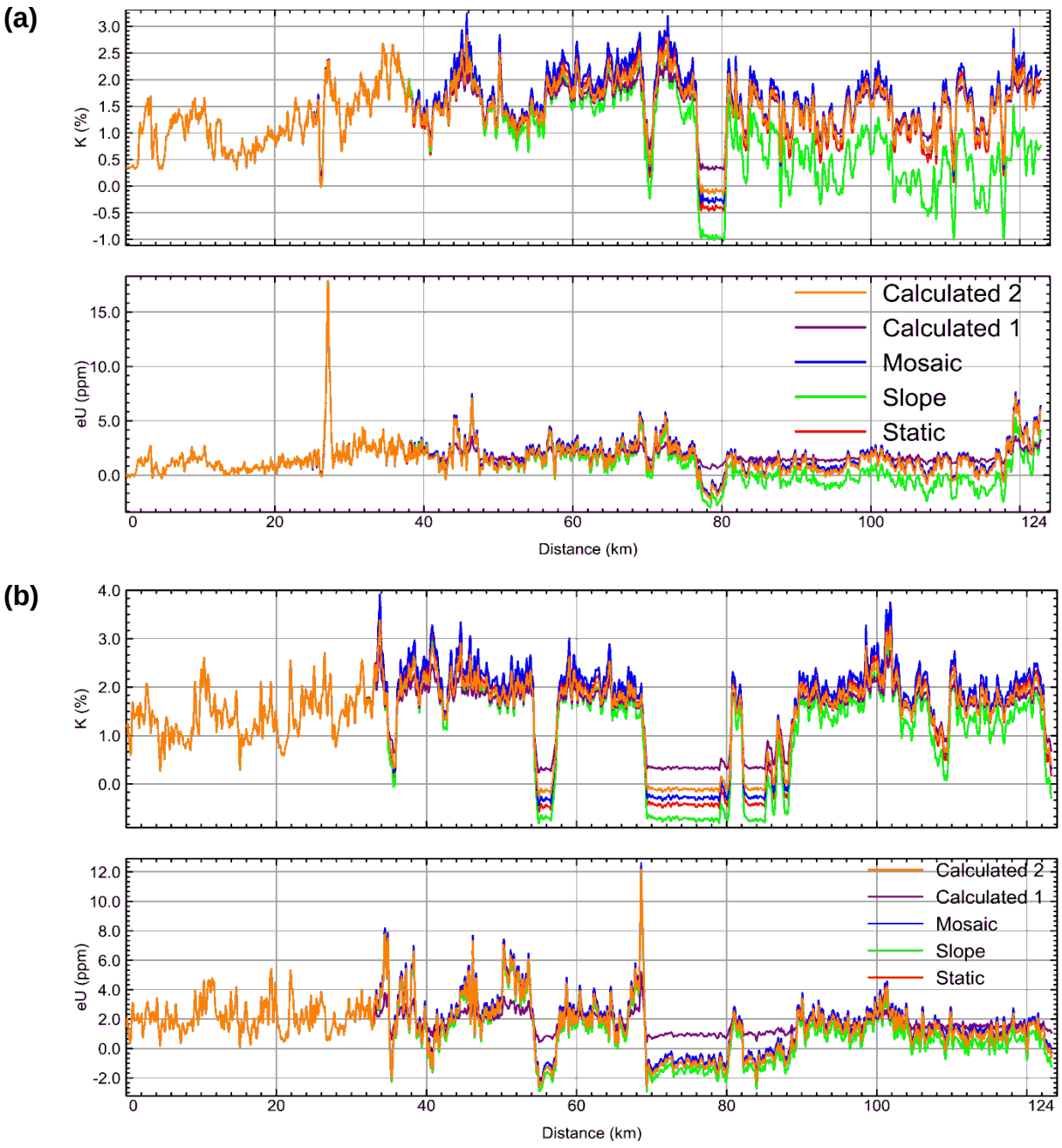

Figure 11: Plots of potassium and uranium extracted from five types of the grids (explained in the text) along profile lines (a) L2 and (b) L3.

Therefore static method of stitching was considered to be appropriate with correction of the grid using regression parameters obtained from the scatter analysis. Potassium and thorium grids of the Fugro survey were modified using regression parameters from Figs 7a and 9a, respectively. Fig. 8 shows a much skewed scatter plot for uranium therefore no correction was applied to uranium grid of the Fugro survey. Applied regression parameters are given in table 3 as well. After modification, the Fugro grids were stitched with NGU grids by removing static trend from Fugro to adjust minor changes along the grid boundaries.

Scatter analysis was also performed in same way for overlapping areas of newly stitched NGU and Fugro grids with SGU grids and shown in Figs. 12-14 for potassium, uranium and thorium. There were no overlapping areas between SGU and Fugro grids. Regression parameters from Figs. 12a, 13a and 14 b were used to

correct mosaiced SGU grids. Corrected SGU grids were stitched with respective stitched NGU and Fugro grids using grid knitting to remove static trend from corrected SGU grids.

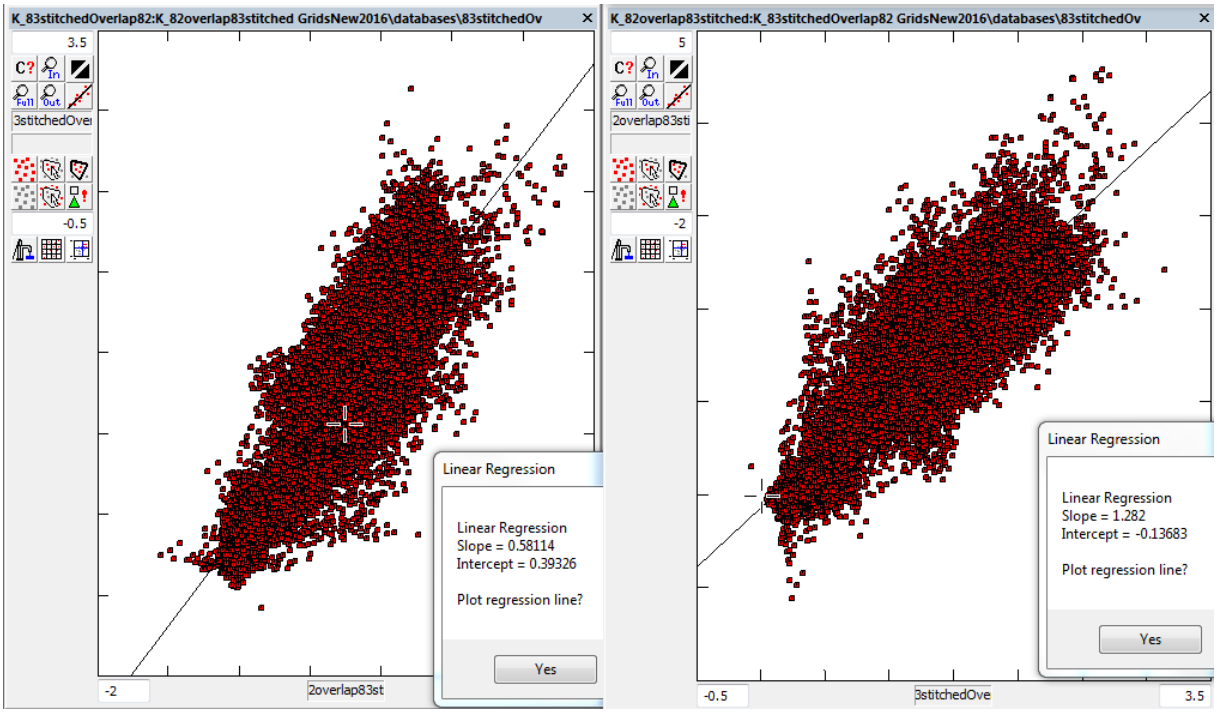

(a) **(b)**

Figure 12: Scatter plot for K between overlapping areas of stitched NGU grid and mosaiced SGU grid with (a) NGU grid on y-axis and SGU grid on x-axis and (b) vice-versa

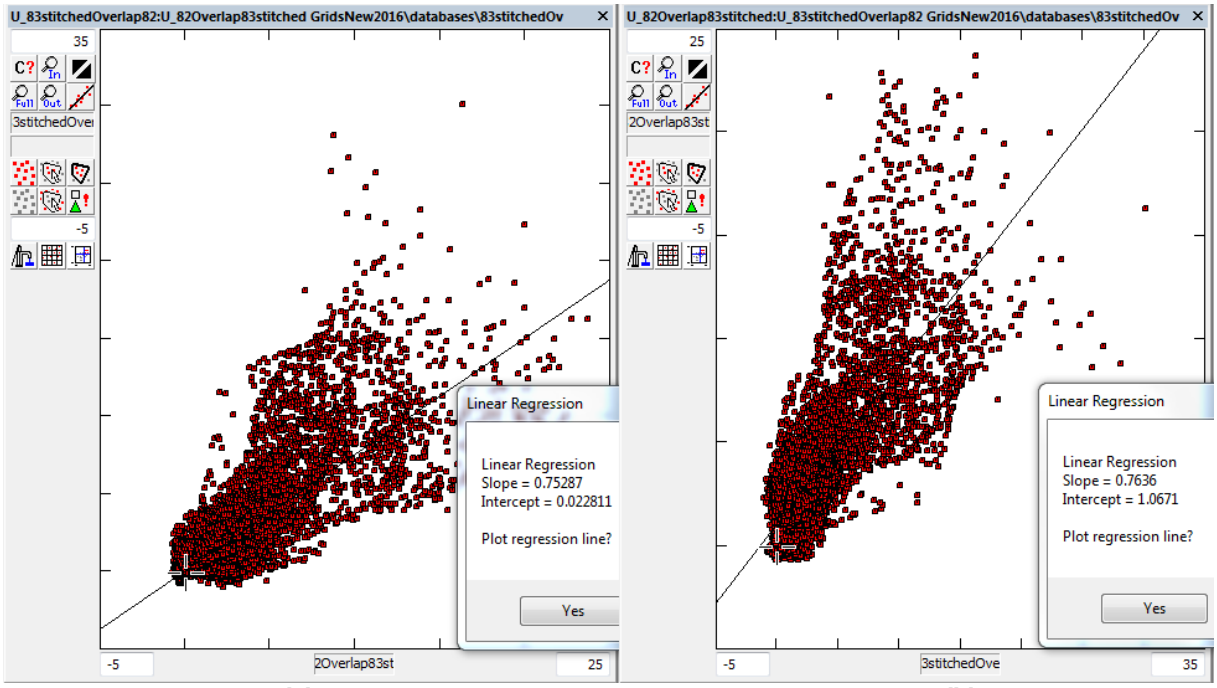

(a) **(b)**

Figure 13: Scatter plot for uranium between overlapping areas of stitched NGU grid and mosaiced SGU grid with (a) NGU grid on y-axis and SGU grid on x-axis and (b) vice-versa.

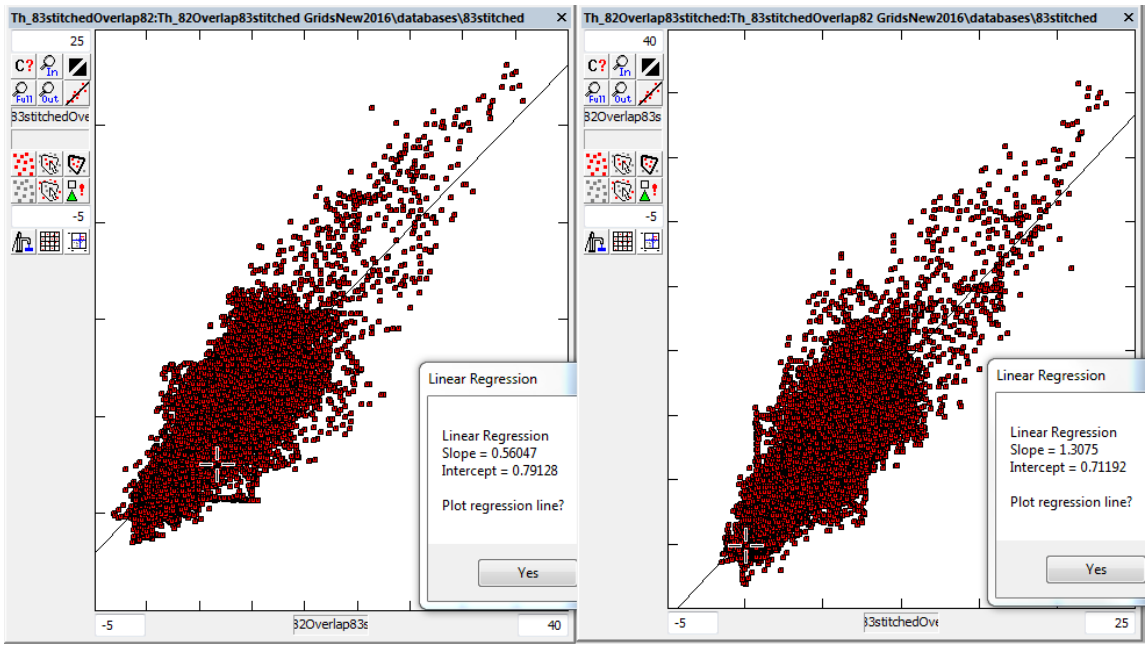

(a) **(b)**

Figure 14: Scatter plot for thorium between overlapping areas of stitched NGU grid and mosaiced SGU grid with (a) NGU grid on y-axis and SGU grid on x-axis and (b) vice-versa

Scatter analysis of the data obtained from overlapping areas of so far stitched grids (NGU, Fugro and SGU) and Larvik are shown in Figs. 15a-17a. Same was performed for Gran and Oppkuven (taking a mosaic of them together) and shown in Figs. 15b to 17b. Ground concentrations were not calculated for Larvik, Gran and Oppkuven surveys and only height corrected counts/second at 60 m height was provided. Therefore scatter analysis by reversing the axes was not performed. Slope values from regression analysis of the scatter plot resulted in calculating sensitivity coefficients at 60 m height (to convert counts/second in the ground concentrations) for these surveys. Sensitivity coefficients at 60 m height for NGU surveys in 2009 and 2011 (Baranwal et al., 2013b) were close to these slope values of the regression analysis. Larvik and mosaiced Gran and Oppkuven were modified using the regression parameters obtained from Figs. 15-17 and then stitched with already stitched NGU, Fugro and SGU grids.

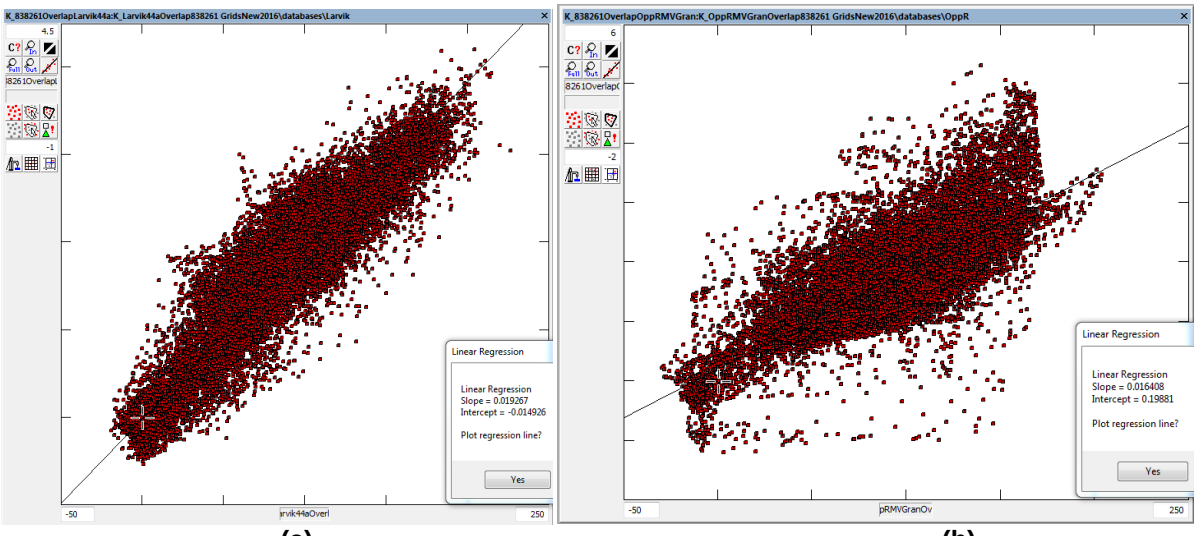

(a) **(b)**

Figure 15: Scatter plot for potassium from overlapping areas of stitched NGU, Fugro, SGU grid with (a) Larvik grid and (b) mosaiced Gran and Oppkuven grid.

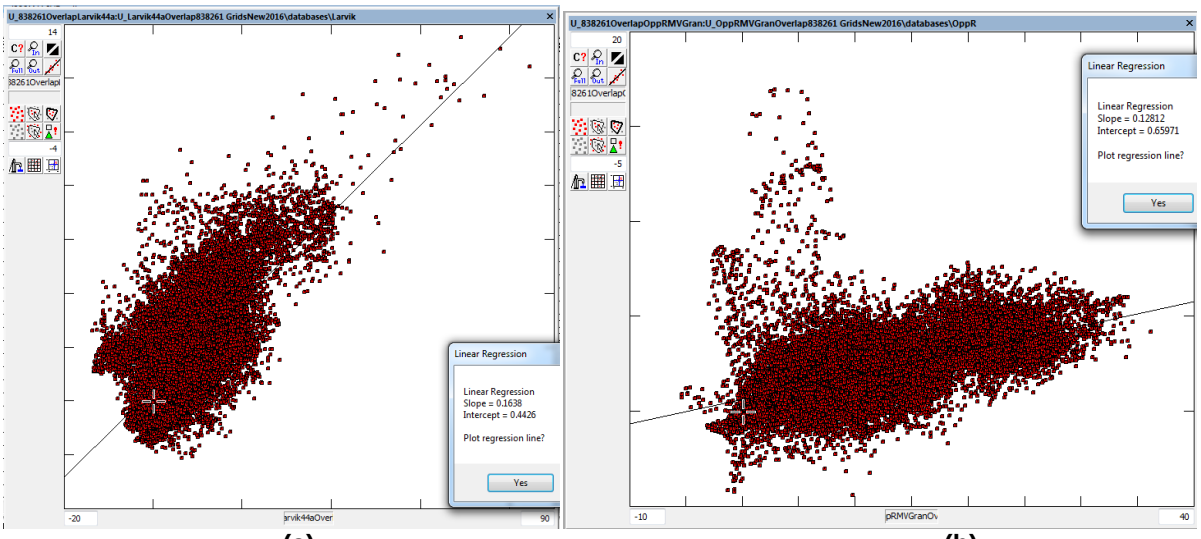

(a) (b)

Figure 16: Scatter plot for uranium from overlapping areas of stitched NGU, Fugro, SGU grid with (a) Larvik grid and (b) mosaiced Gran and Oppkuven grid.

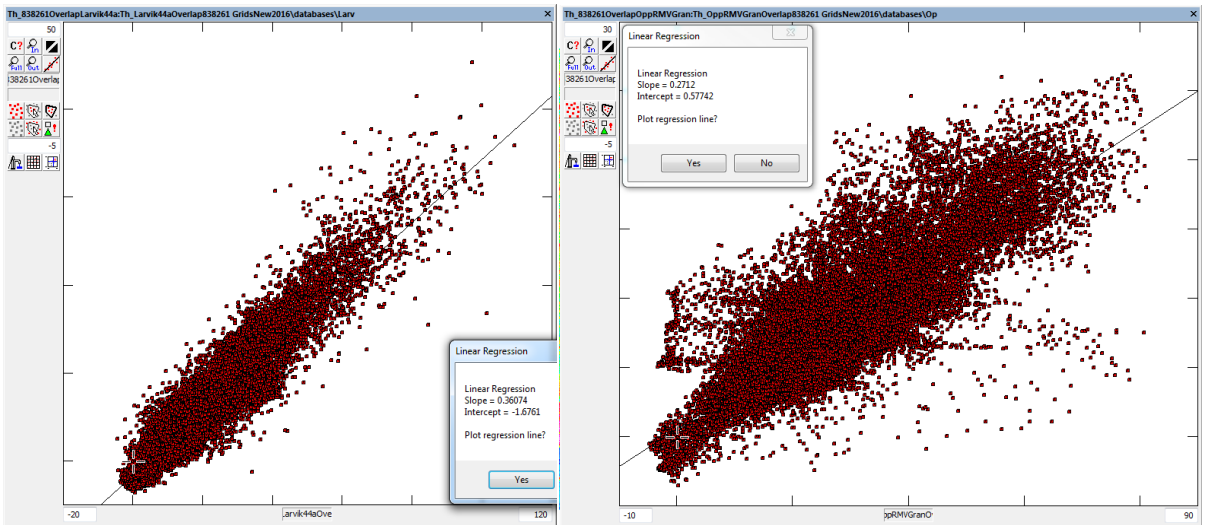

(a) (b)

Figure 17: Scatter plot for thorium from overlapping areas of stitched NGU, Fugro, SGU grid with (a) Larvik grid and (b) mosaiced Gran and Oppkuven grid.

After stitching, uranium grid showed a general higher concentration in Gran and Oppkuven area. Scatter plot of uranium for Oppkuven and Gran (Fig. 16b) was not oval-shaped therefore regression parameters from Larvik were used. Same scatter plot analysis and grid knitting process was repeated to stitch Sandefjord and Nordagutu grids. Scatter analysis plots are shown in Figs. 18-20 for Sandefjord and in Figs 21-23 for Nordagutu. Accepted regression parameters for Sandefjord for K, eU and eTh were from Figs. 18a, 19b and 20a, respectively and for Nordagutu for K, eU and eTh were from Figs. 21a, 22b and 23c, respectively. Used regression parameters are mentioned in table 3 as well.

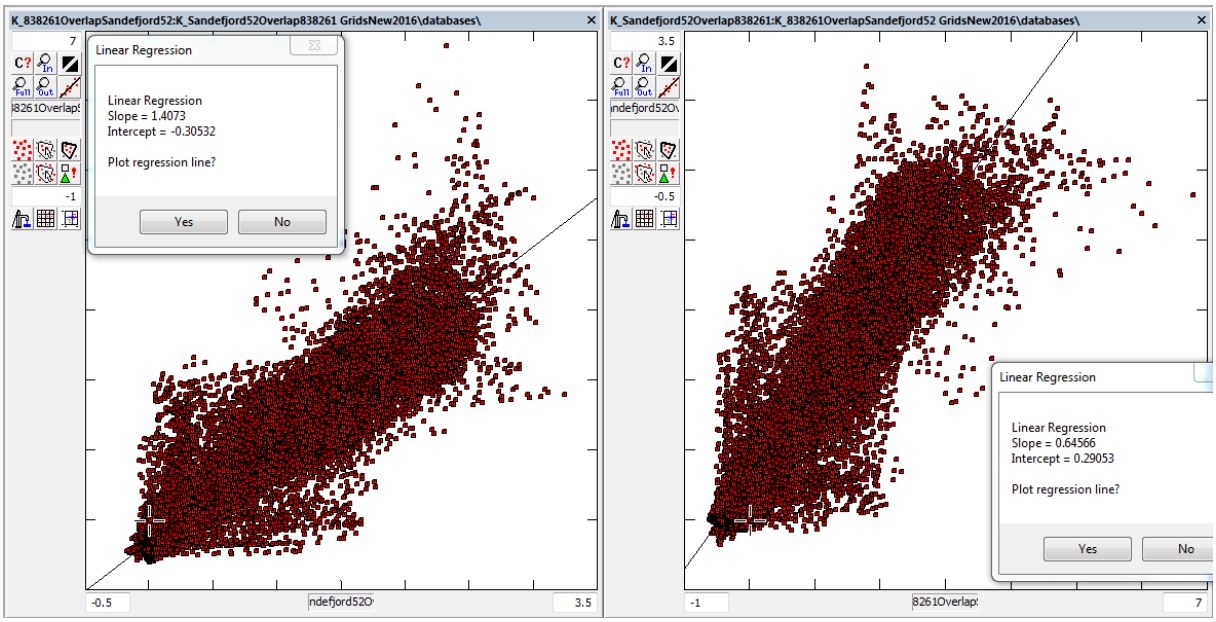

(a) **(b)**

Figure 18: Scatter plot for potassium from overlapping areas of stitched NGU, Fugro, SGU, Larvik, Gran, Oppkuven grid and Sandefjord grid with (a) big stitched grid data on y-axis and Sandefjord grid data on x-axis and (b) vice-versa.

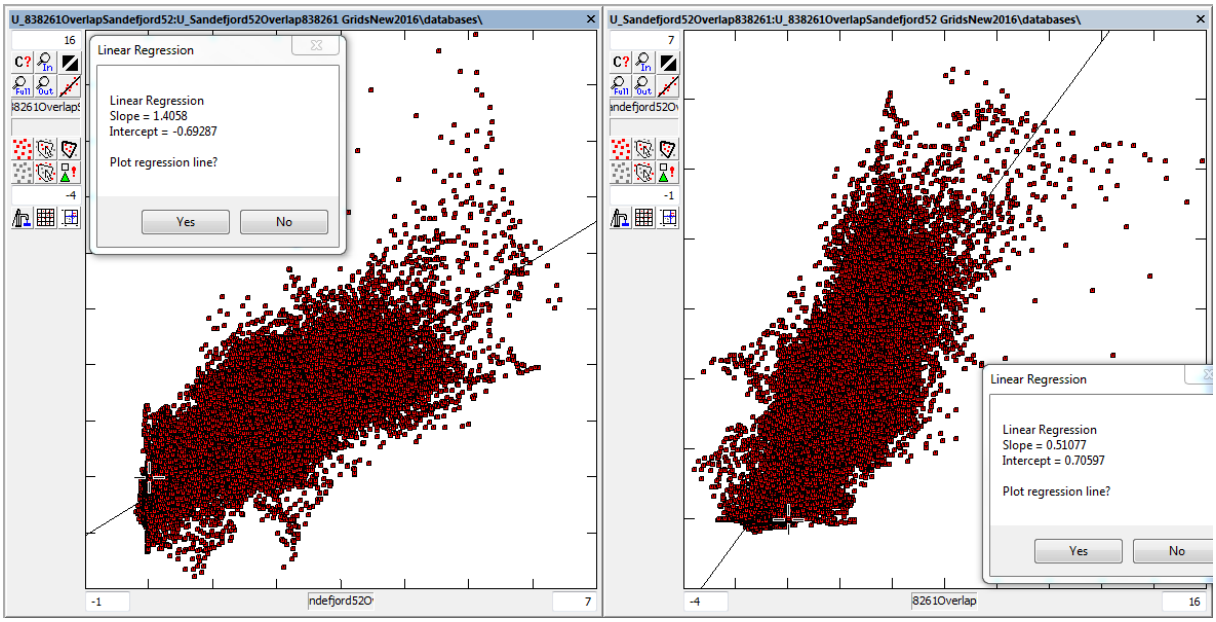

(a) **(b)**

Figure 19: Scatter plot for uranium from overlapping areas of stitched NGU, Fugro, SGU, Larvik, Gran, Oppkuven grid and Sandefjord grid with (a) big stitched grid data on y-axis and Sandefjord grid data on x-axis and (b) vice-versa.

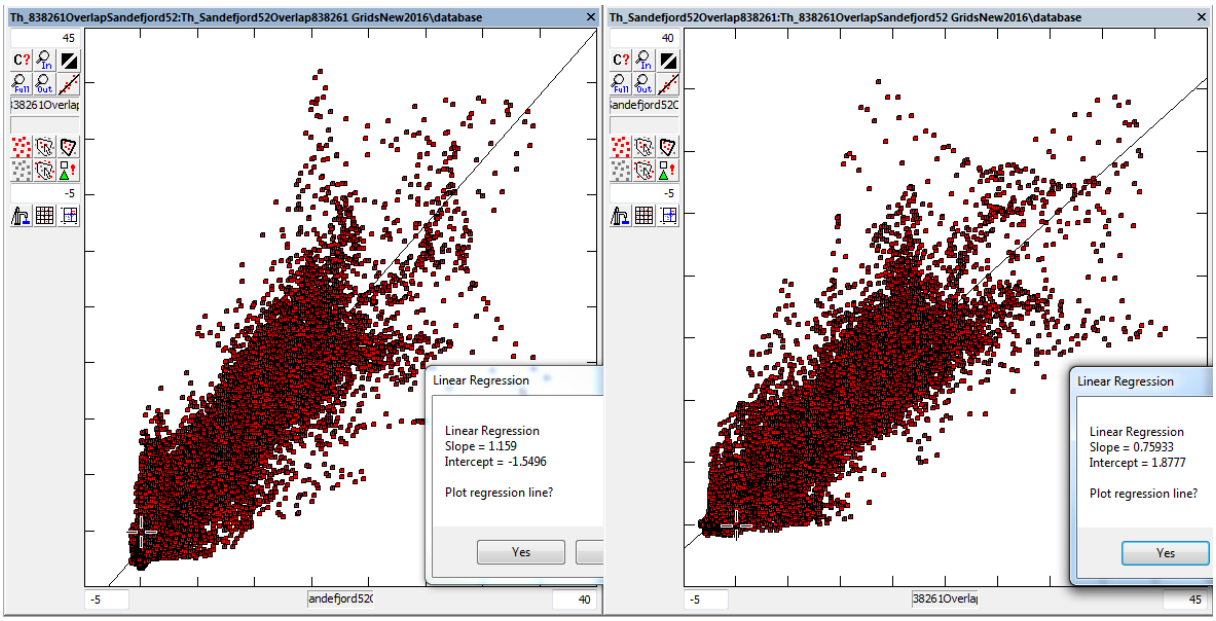

(a) (b)

Figure 20: Scatter plot for thorium from overlapping areas of stitched NGU, Fugro, SGU, Larvik, Gran, Oppkuven grid and Sandefjord grid with (a) big stitched grid data on y-axis and Sandefjord grid data on x-axis and (b) vice-versa.

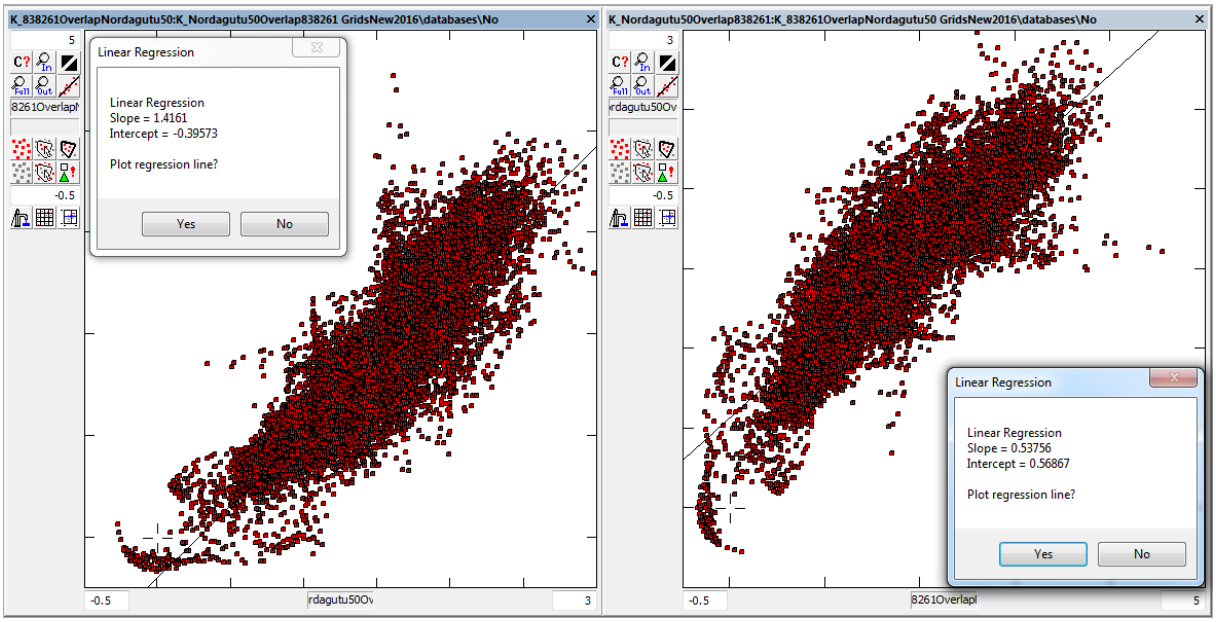

(a) (b)

Figure 21: Scatter plot for potassium from overlapping areas of stitched NGU, Fugro, SGU, Larvik, Gran, Oppkuven grid and Nordagutu grid with (a) big stitched grid data on y-axis and Nordagutu grid data on x-axis and (b) vice-versa.

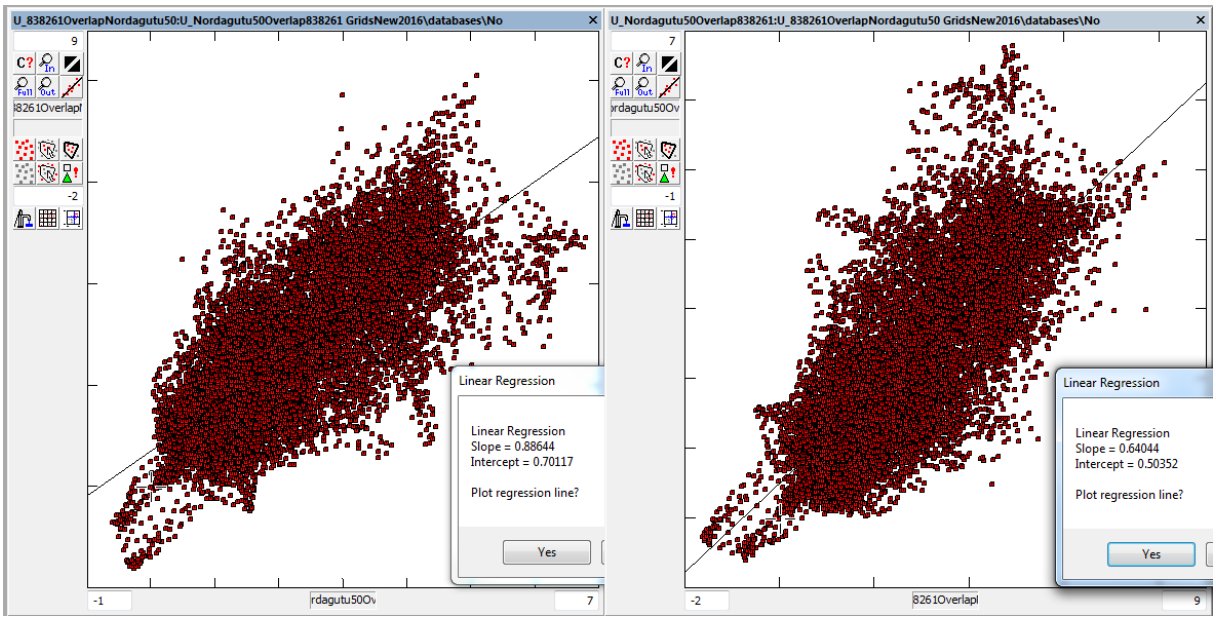

(a) (b)

Figure 22: Scatter plot for uranium from overlapping areas of stitched NGU, Fugro, SGU, Larvik, Gran, Oppkuven grid and Nordagutu grid with (a) big stitched grid data on y-axis and Nordagutu grid data on x-axis and (b) vice-versa.

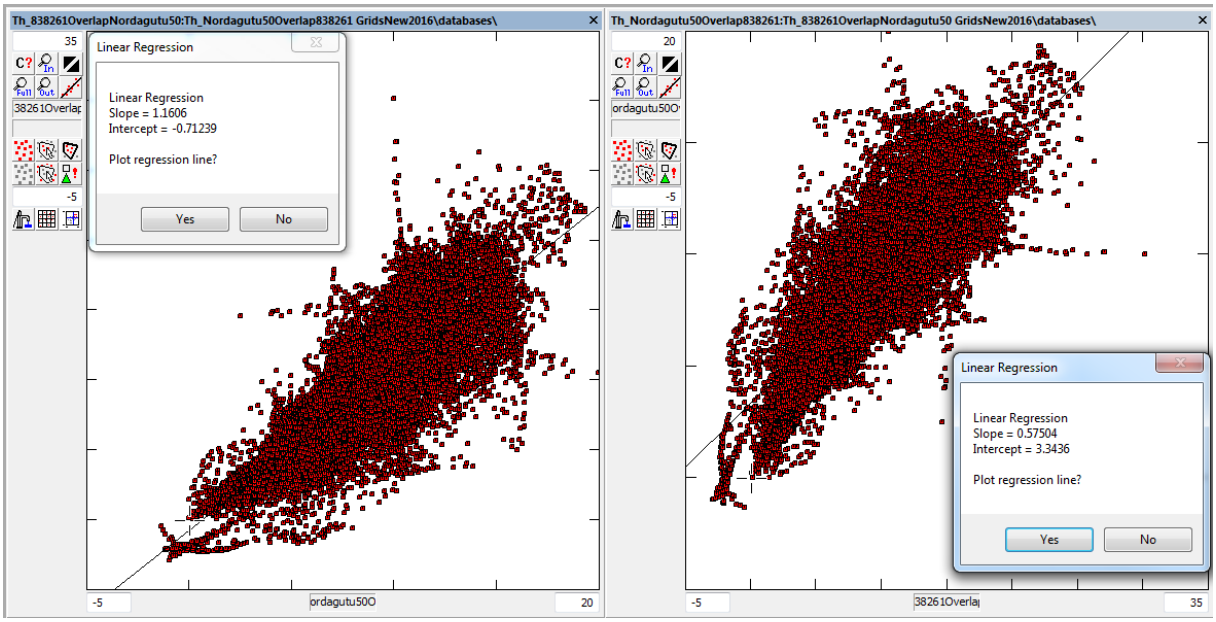

(a) (b)

Figure 23: Scatter plot for thorium from overlapping areas of stitched NGU, Fugro, SGU, Larvik, Gran, Oppkuven grid and Nordagutu grid with (a) big stitched grid data on y-axis and Nordagutu grid data on x-axis and (b) vice-versa.

After stitching of Sandfjord and Nordagutu grids, same process was repeated to stitch Hurdal and Siljan grids. Scatter analysis plots are shown in Figs. 24-26 for Hurdal and in Figs 27-29 for Siljan. Accepted regression parameters for Hurdal were from Figs. 24a-26a and for Siljan were from Figs. 27a-29a. After stitching, uranium in Hurdal area showed a general higher concentration than the neighboring region. Most of the uranium data was in lower concentration area of the scatter plot and the area of the high density data looked more irregular-shaped than an expected oval-shaped (Fig. 25a). Sandefjord survey was performed in 2000, same year of Hurdal survey, therefore, regression parameters of Sandefjord for uranium were used to correct Hurdal uranium.

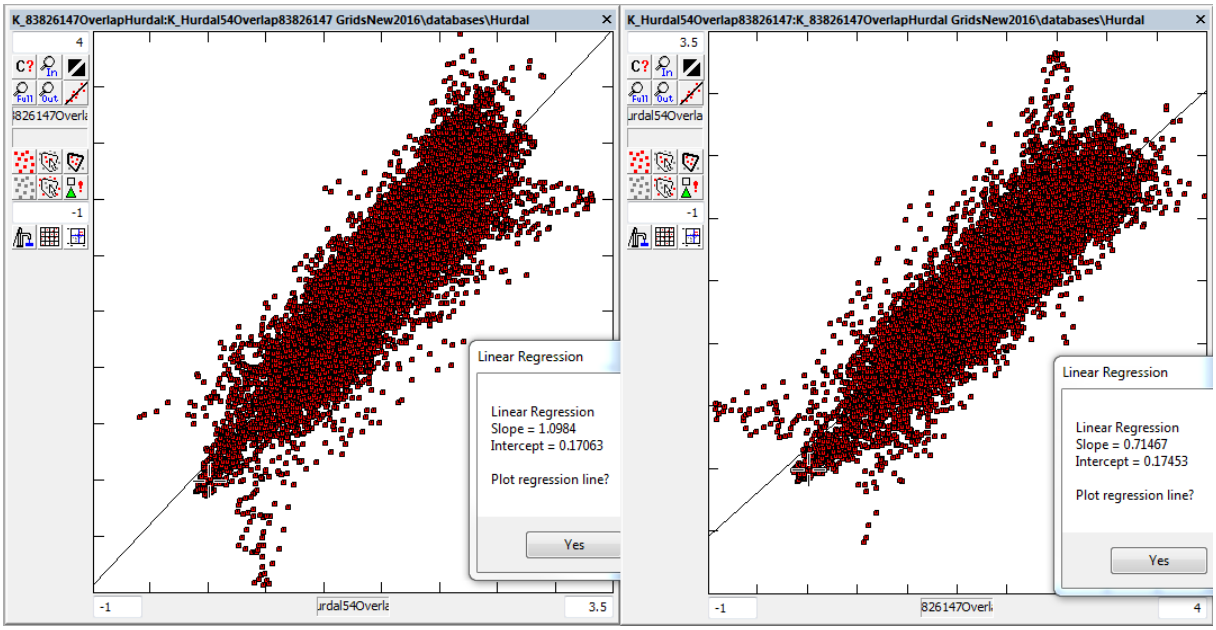

(a) (b)

Figure 24: Scatter plot for potassium from overlapping areas of stitched NGU, Fugro, SGU, Larvik, Gran, Oppkuven, Sandefjord, Nordagutu grid and Hurdal grid with (a) big stitched grid data on y-axis and Hurdal grid data on x-axis and (b) vice-versa.

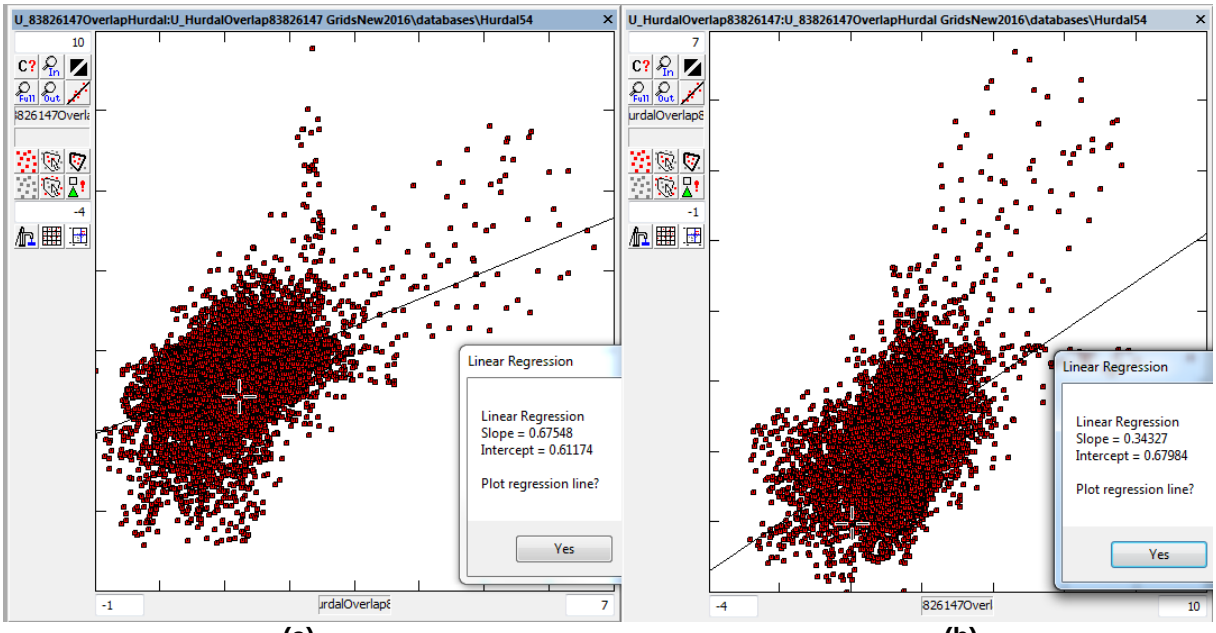

(a) (b)

Figure 25: Scatter plot for uranium from overlapping areas of stitched NGU, Fugro, SGU, Larvik, Gran, Oppkuven, Sandefjord, Nordagutu grid and Hurdal grid with (a) big stitched grid data on y-axis and Hurdal grid data on x-axis and (b) vice-versa.

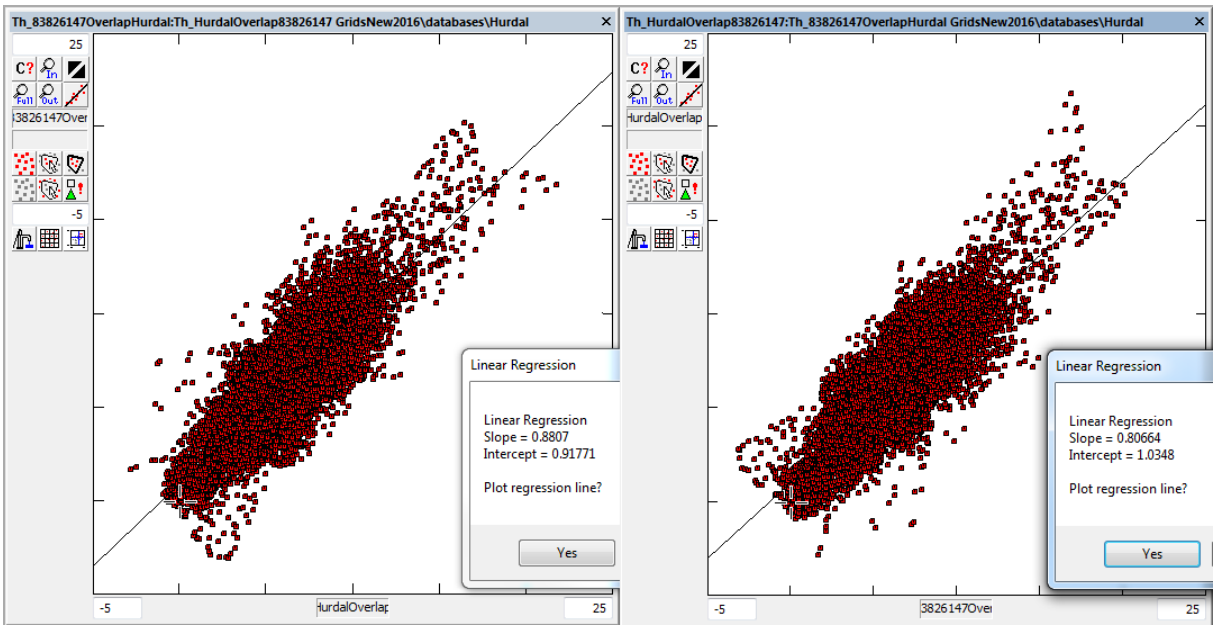

(a) (b)

Figure 26: Scatter plot for thorium from overlapping areas of stitched NGU, Fugro, SGU, Larvik, Gran, Oppkuven, Sandefjord, Nordagutu grid and Hurdal grid with (a) big stitched grid data on y-axis and Hurdal grid data on x-axis and (b) vice-versa.

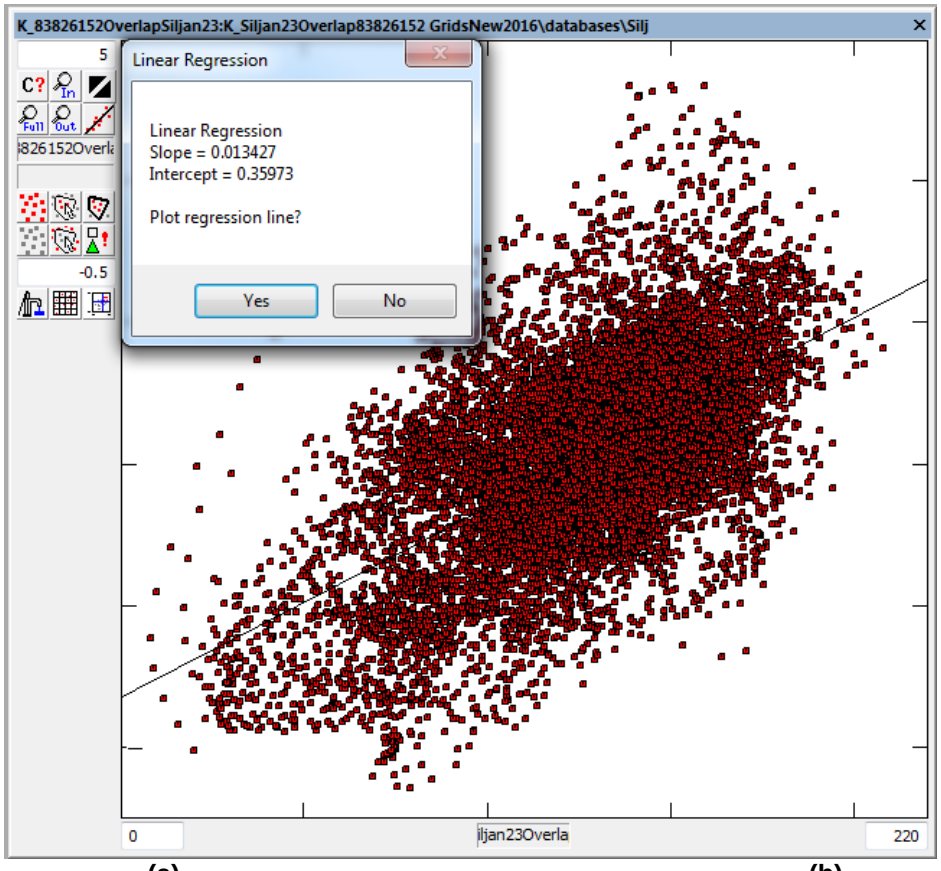

(a) (b)

Figure 27: Scatter plot for potassium from overlapping areas of stitched NGU, Fugro, SGU, Larvik, Gran, Oppkuven, Sandefjord, Nordagutu grid and Siljan grid with big stitched grid data on y-axis and Siljan grid data on x-axis.

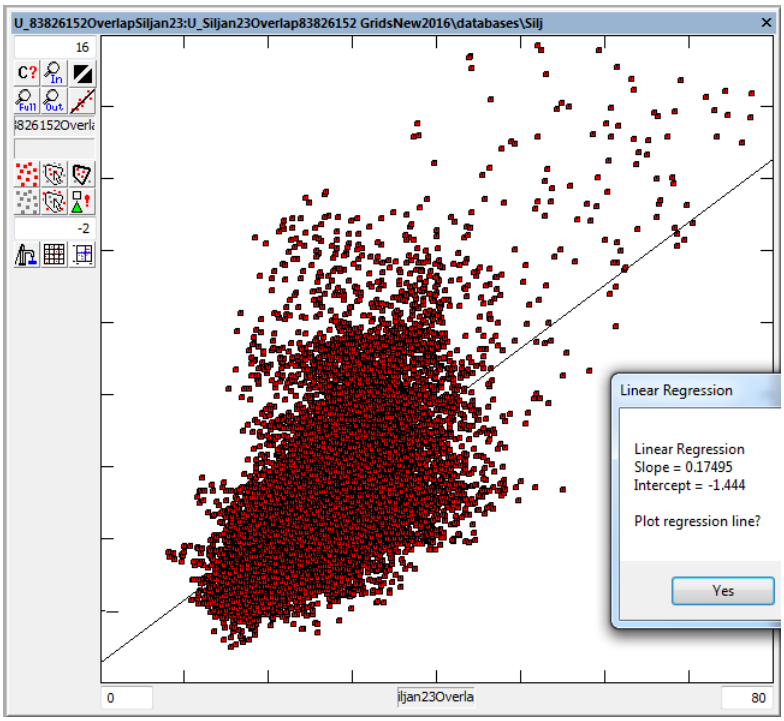

(a) (b)

Figure 28: Scatter plot for uranium from overlapping areas of stitched NGU, Fugro, SGU, Larvik, Gran, Oppkuven, Sandefjord, Nordagutu grid and Siljan grid with big stitched grid data on y-axis and Siljan grid data on x-axis.

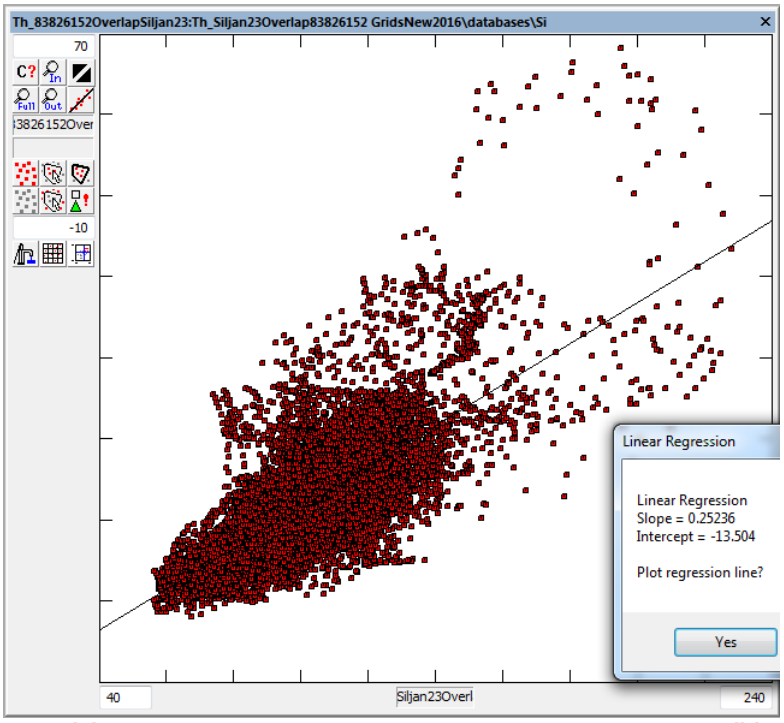

(a) (b)

Figure 29: Scatter plot for thorium from overlapping areas of stitched NGU, Fugro, SGU, Larvik, Gran, Oppkuven, Sandefjord, Nordagutu grid and Siljan grid with big stitched grid data on y-axis and Siljan grid data on x-axis.

Final stitched grids with cell size 50 x 50 meters for K, eU and eTh with shading are shown in Figs. 30-32, respectively. A ternary image using the grids of K, eU and eTh was also derived and can be obtained on request.

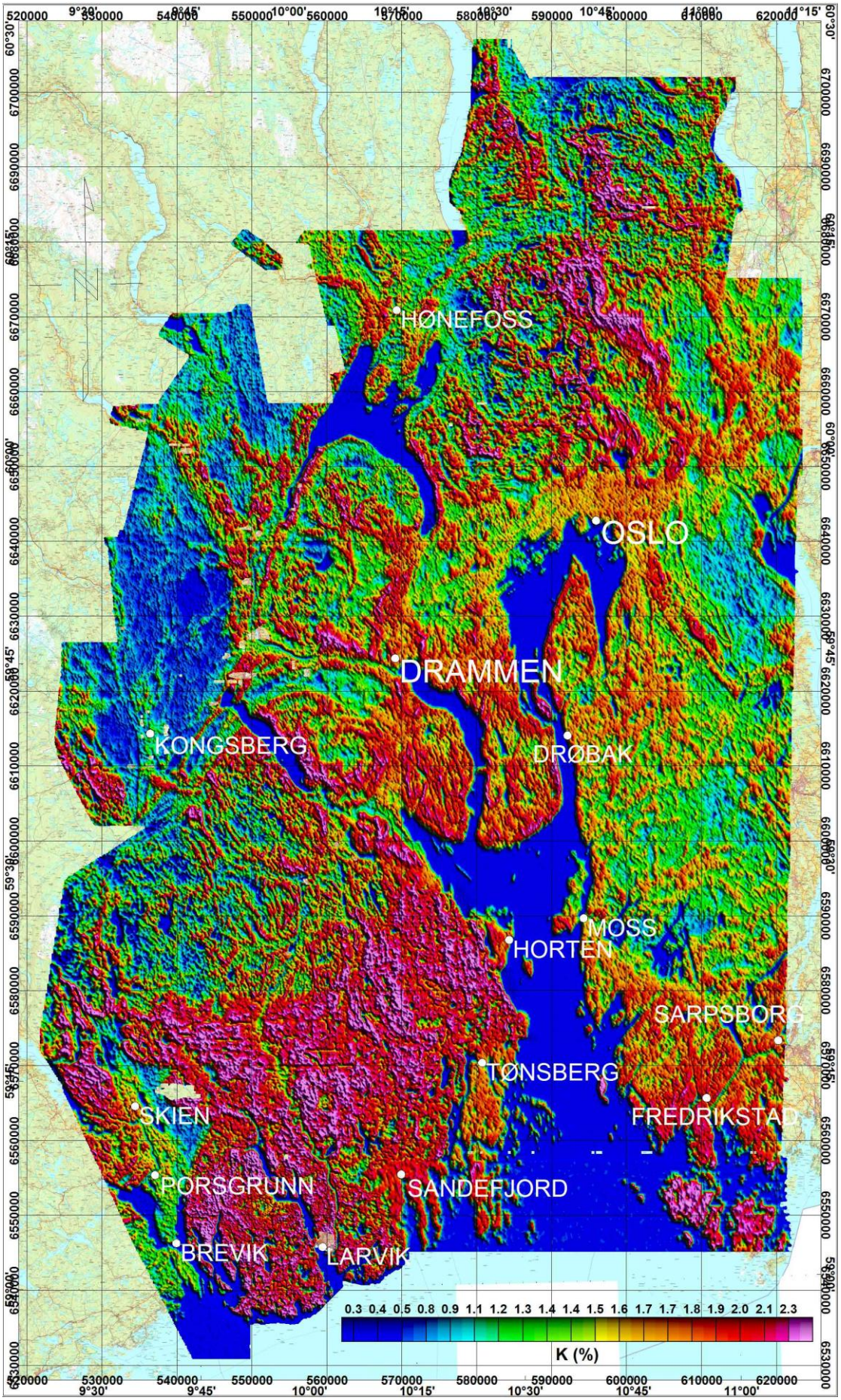

Figure 30: Stitched potassium (K) ground concentration map from the Oslofjord area.

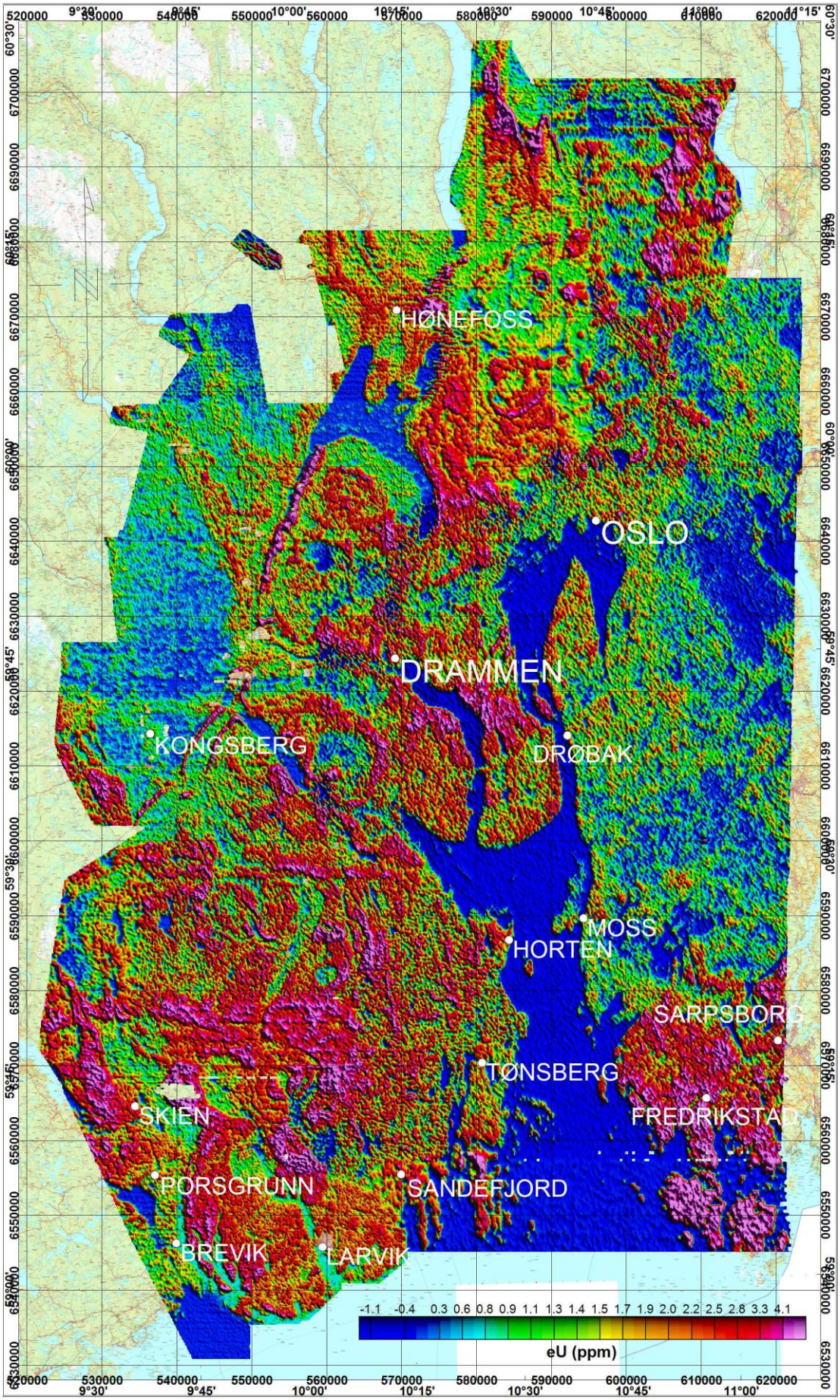

Figure 31: Stitched uranium (eU) ground concentration from the Oslofjord area.

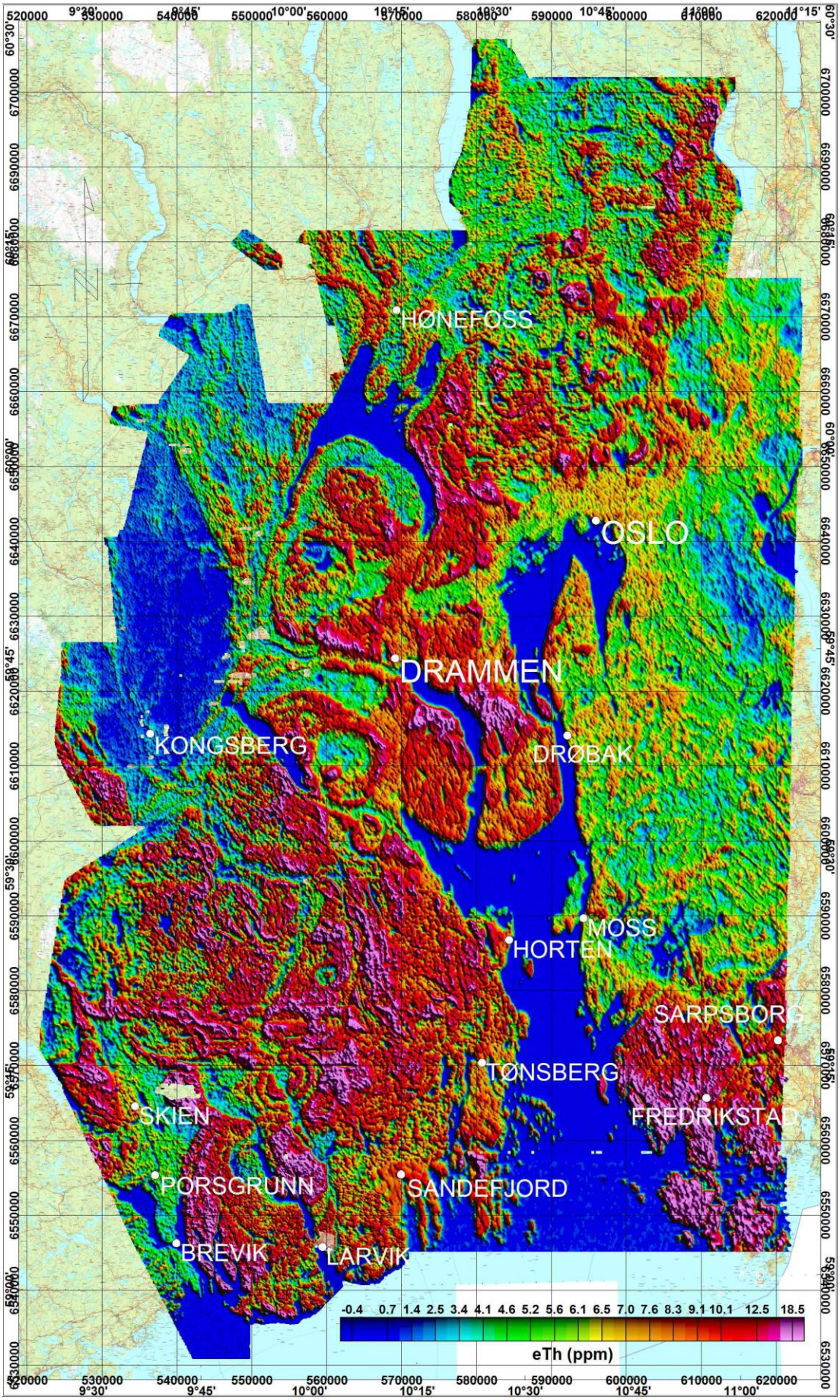

Figure 32: Stitched thorium (eTh) ground concentration from the Oslofjord area.

5. DISCUSSION AND CONCLUDING REMARKS

Various grids for magnetic and radiometric data were stitched together from airborne surveys performed during 1981-2011. Stitching of magnetic data was straightforward. It was done by suture method of automatic stitching available in gridknit software of Geosoft.

Stitching of radiometric data could not be performed automatically because some of earlier surveys were not calibrated. Some of the surveys had counts of gamma radiations for K, eU and eTh windows as gridded data. There were no aircraft background correction, cosmic correction, height attenuation and sensitivity coefficients available from these surveys. Some of these grids had along-line leveling errors, and therefore, some efforts were made to micro-level such grids to remove these errors. Fugro had used NASVD to remove random noise from data which matched better with NGU and SGU data compared to the one without NASVD. To bring all the data from different surveys at same level of ground concentration, scatter analysis of the overlapping areas of various grids was performed. Slope and intercept values were obtained by regression analysis of the plot. These regression parameters were used to bring two grids at similar level of the concentration and then all the grids were stitched together one by one to obtain the final grid. The scatter analysis didn't give always a good linear relation especially between NGU and Fugro data for uranium. Sometime there were not sufficient overlapping areas and parameters of regression analysis could be inaccurate.

It can be seen from stitched magnetic grid that the quality of the stitching is quite good and no level difference from one survey to other is observed. Radiometry grids also seem good except some areas where along-line leveling errors could not be removed. A critical review of the individual radiometry grids indicate some minor level differences from one grid to other on all three elements, and also along-line level errors within Siljan, Hurdal survey areas which were even more in original grid before stitching. Re-processing of the data with correct coefficients and thorough leveling is required to do further improvements in the quality of stitched grid.

It is observed from scatter analysis that NGU grid was around 1.6 times higher in concentration of potassium and around 1.3 times higher in concentration of thorium in the overlapping areas of SGU and Fugro grids. Uranium was found 1.3 times higher in NGU grid than SGU however Fugro grid could not give a good linear relationship with NGU grid for uranium. Some of the other survey areas were deviated from good linear relationship in the regression analysis and some showed a higher concentration compared to the neighboring areas. Then parameters from other survey area performed in the same year were used to correct it.

6. REFERENCES

Baranwal, V.C. Olesen, O. & Rønning J.S. 2013a: Preparation of action map for tunnel planning in the South-Eastern Norway: Mapping of deep weathered weak zones, NGU report 2013.003, 27 pp.

Baranwal V.C., Rodionov A., Ofstad F., Koziel J. & Lynum R. 2013b: Helicopter-borne magnetic, electromagnetic and radiometric geophysical surveys in the Kongsberg region: Krøderen, Sokna, Hønefoss, Kongsberg and Numedalen, NGU report 2013.029, 53 pp.

Beard, L.P. 1998: Data acquisition and processing - helicopter geophysical survey, Oppkuven and Gran, 1997. *NGU Report 98.079*, 20 pp.

Beard, L.P. 1999: Data acquistion and processing - helicopter geophysical survey, Larvik, 1998. *NGU Report 99.026*, 13 pp.

Beard, L.P. & Rønning, S. 1997: Data aquisition and processing report – helicopter geophysical survey, Krokskogen. *NGU Report 97.134*, 9 pp.

Beard, L.P. & Lutro, O. 2000: Airborne geophysics and infrastructure planning – A case study. *Journal of Environmental and Engineering Geophysics 5,* 1-10.

Beard, L.P. & Mogaard, J.O. 2001: Data acquisition and processing – helicopter geophysical survey, Hurdal, 2000. *NGU Report 2001.018,* 16 pp.

Fugro Airborne Surveys 2003: Logistics report, fixed-wing borne magnetic, radiometric and VLF-EM survey in the Oslo region, southern Norway. *Report FCR 2241*, 124 pp.

Geosoft, 2010a: *Montaj MAGMAP filtering, 2-D frequency domain processing of potential field data, Extension for Oasis Montaj v7.1.* Geosoft Incorporation, 72 pp.

Geosoft, 2010b: *Montaj GridKnit, Grid stitching extension for OASIS Montaj v7.1, Tutorial and user guide,* Geosoft Incorporation, 28 pp.

Minty, B. & McFadden, P., 1998: Improved NASVD smoothing of airborne gamma-ray spectra. *Exploration Genphysics* 29, 516-523.

Håbrekke, H. 1982: Magnetiske-, elektromagnetiske-, VLF- og radiometriske målinger fra helikopter over et område vest for Tønsberg, Vestfold og Telemark fylker. *NGU Report 1835,* 13 pp.

Mogaard, J.O. 1998: Geofysiske målinger fra helikopter ved Larvik, Vestfold. NGU Report 98.021, 11 pp.

Mogaard, J.O. 2001: Geofysiske målinger fra helikopter ved Sandefjord, Vestfold 2000. NGU Report 2001.003, 12 pp.

Mogaard, J.O. 2006: Data acquisition and processing - Helicopter Geophysical Survey, Bamle, Ertlien and Sigdal 2005. NGU Report 2006.021, 11 pp.

Mogaard, J.O. & Beard, L.P. 2000: Geofyiske målinger fra helicopter ved Skien, Telemark 1999. NGU Rapport 2000.031, 12 pp.

SGU 2009: Produktion av flyggeofysiska mätdata för projekt SPAS-09. Sveriges geologiska undersökning's slutrapport.

GEOLOGICAL
SURVEY OF
NORWAY

· NGU ·

Geological Survey of Norway
PO Box 6315, Sluppen
N-7491 Trondheim, Norway

Visitor address
Leiv Eirikssons vei 39
7040 Trondheim

Tel (+ 47) 73 90 40 00
E-mail ngu@ngu.no
Web www.ngu.no/en-gb/